

# A unified theory of feature learning in RNNs and DNNs

Jan P. Bauer<sup>1</sup> Kirsten Fischer<sup>2</sup> Moritz Helias<sup>2</sup> Agostina Palmigiano<sup>1</sup>

## Abstract

Recurrent and deep neural networks (RNNs/DNNs) are cornerstone architectures in machine learning. Remarkably, RNNs differ from DNNs only by weight sharing, as can be shown through unrolling in time. How does this structural similarity fit with the distinct functional properties these networks exhibit? To address this question, we here develop a unified mean-field theory for RNNs and DNNs in terms of representational kernels, describing fully trained networks in the feature learning ( $\mu$ P) regime. This theory casts training as Bayesian inference over sequences and patterns, directly revealing the functional implications induced by the RNNs' weight sharing. In DNN-typical tasks, we identify a phase transition when the learning signal overcomes the noise due to randomness in the weights: below this threshold, RNNs and DNNs behave identically; above it, only RNNs develop correlated representations across timesteps. For sequential tasks, the RNNs' weight sharing furthermore induces an inductive bias that aids generalization by interpolating unsupervised time steps. Overall, our theory offers a way to connect architectural structure to functional biases.

## 1. Introduction

Understanding how neural networks learn useful representations from data remains a central question in machine learning theory. While recent work has studied feature learning in DNNs (Yang & Hu, 2020; Bordelon & Pehlevan, 2022b; Cui et al., 2023), the corresponding theory for RNNs is far less developed. RNNs process sequences by repeatedly applying the same transformation over time, so that each new hidden state is computed using the same set of recurrent

<sup>1</sup>Gatsby Computational Neuroscience Unit, UCL, London, UK <sup>2</sup>IAS-6, Forschungszentrum Juelich, Juelich, Germany. Correspondence to: Jan P. Bauer, Agostina Palmigiano <{j.bauer, a.palmigiano}@ucl.ac.uk>.

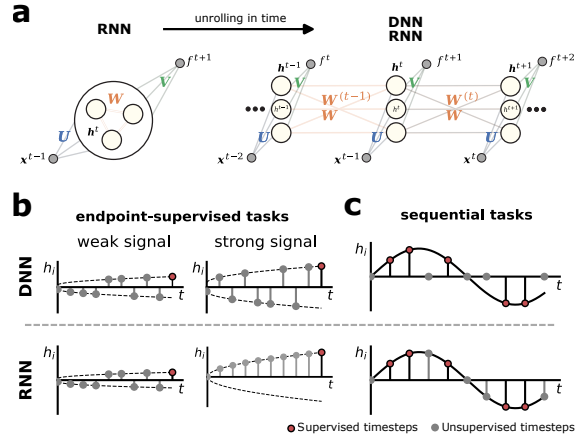


**Figure 1. Graphical abstract: RNNs resemble DNNs after unrolling-in-time, but differ functionally depending on signal strength and tasks.** **a)** Recurrent neural network (RNN, left) and its unrolling-in-time representation (right): the same recurrent weights  $W$  are shared across timesteps. **b)** *Endpoint-supervised tasks*: Supervision target at the last layer (red) affects hidden layer representation (gray), but only in the RNN and for sufficient signal strength induces a phase transition towards temporal coherence. **c)** *Sequential tasks*: The RNNs weight sharing induces a temporally coherent inductive bias that facilitates generalization from supervised (red) to unsupervised timepoints (gray), whereas the DNN exhibits “regression to the mean” for unsupervised points due to an effectively white prior.

weights  $W$ . If we “unroll” this computation in time, the RNN can be viewed as a deep feedforward network whose layers correspond to timesteps. From this view, the two network architectures appear remarkably similar (Fig. 1). However, a difference is that the weights are shared across all layers (timesteps) in the RNN, whereas a standard DNN has layer-specific weights. It is so far unknown how weight sharing affects computation: are the extra, untied parameters of a DNN always advantageous, or can the inductive bias imposed by weight sharing actually improve learning by better aligning the model with the structure of a task?

Our key contributions towards this question are:

- We develop a unified mean-field theory for RNNs and DNNs in terms of representational kernels, describing trained networks after convergence of Langevin stochastic gradient descent in the feature learning ( $\mu$ P) regime

regime. This theory casts network training as Bayesian inference over timesteps and patterns, revealing the functional implications of their architectural structure.

- For tasks that are typical for DNNs (“*endpoint-supervised*” tasks), we analytically show that even within  $\mu$ P scaling, different phases of feature learning exist. Below a critical signal strength, the representational kernels of RNNs and DNNs coincide, although they differ from the kernels obtained in a lazy learning phase (NNGP), which characterize initialization. Beyond a critical signal strength, however, the RNN’s representation enters a *temporally coherent* phase that is absent in the DNN.
- For tasks that are typical for RNNs (“*sequential*” tasks), we show how the RNN’s weight sharing induces an inductive bias that enables more sample-efficient learning. This implies a functional advantage beyond the representational changes of the endpoint-supervised case, and underlines that task-model alignment not only depends on expressivity, but also on adaptivity to task structure.

The code to reproduce all figures is available at [github.com/japhba/temporal-feature-learning](https://github.com/japhba/temporal-feature-learning).

## 2. Related work

**Probabilistic descriptions of neural networks.** The study of feedforward neural networks in the infinite-width limit has a rich history, beginning with the connection to Bayesian inference (Neal, 1996; Lee et al., 2018). These foundational works established that infinitely wide neural networks with random weights under the standard parametrization (SP, all weights scale as  $1/\sqrt{\text{width}}$ ) converge to Gaussian processes. More recently, this line of work has been generalized using mean-field methods to account for feature learning either by adopting  $\mu$ P scaling (Yang & Hu (2020), readout weights scale as  $1/\text{width}$ ), or by considering proportional limits of width and number of data samples. Such theories have been formulated in terms of adaptive weight scales Li & Sompolsky; Ariosto et al.; Pacelli et al., task-aligned readout weights (van Meegen & Sompolsky, 2025), or kernel matrices (Seroussi & Ringel, 2021; Zavatone-Veth & Pehlevan, 2021; Fischer et al., 2024; Lauditi et al., 2025), providing a probabilistic description of representations that goes beyond dynamics near initialization as described by the neural tangent kernel (NTK) (Jacot et al., 2018). We here develop a generalization of such kernel theories to RNNs in a way that treats RNNs and DNNs on equal footing.

**Bayesian inference in state-space models.** Our approach to analyzing recurrent networks directly connects

to Bayesian inference in classical probabilistic models. In particular, for linear activation, the RNN architecture we consider is identical to a linear Gaussian state-space model with vanishing noise in the forward pass (Kalman, 1960). Whereas these models consider inference at fixed weights via Kalman filtering, we here consider a posterior over weights due to training as well, leading to a more general theory.

**Theory of recurrent neural networks.** The dynamics of randomly-coupled recurrent neural networks have been studied extensively. Dynamical mean field theory has been derived in networks with random unstructured (Sompolsky et al., 1988; Molgedey et al., 1992; Toyoizumi & Abbott, 2011b), excitatory and inhibitory (Kadmon & Sompolsky, 2015; Sanzeni et al., 2023; Mastrogiosepe & Ostoic, 2017) and low-rank (Mastrogiosepe & Ostoic, 2019; Landau & Sompolsky, 2018) connectivity (Schuecker et al., 2018; Segadlo et al., 2022; Schuessler et al., 2024), including their response to perturbations (Sanzeni et al., 2023; Nguyen et al., 2025; Palmigiano et al., 2023) and computational properties (such as memory (Toyoizumi & Abbott, 2011a; Schuecker et al., 2018; Pereira-Obilinovic et al., 2023)). The study of learning in RNNs is less thoroughly explored. The recurrent neural tangent kernel (RNTK) (Alemohammad et al., 2021) extends the NTK framework (Jacot et al., 2018) to recurrent architectures, providing insights into their training dynamics in the infinite-width lazy training regime. Proca et al. (2025); Bordelon & Pehlevan (2025) analyzed the learning *dynamics* in recurrent linear networks in the balanced regime. Bordelon et al. (2024) presented ideas to study learning as Bayesian inference in RNNs in continuous time with a leak term (Amari, 1972).

**Generalization, architectural inductive biases and feature learning.** Kernel methods have been employed to study generalization (Canatar et al., 2021; Simon et al., 2023; van Meegen & Sompolsky, 2025; Rubin et al., 2025), with tight links to the training of neural networks and the role of inductive biases (Aiudi et al., 2025). Meanwhile, other work has explored the impact of initialization necessary for feature learning, in particular the role of small initialization (Saxe et al., 2013; Atanasov et al., 2021; Kunin et al., 2024; Tu et al., 2024). We here study feature learning in terms of structured updates to the kernel’s eigenvectors, highlighting the effects of architecture and initialization.

**Learning dynamics versus convergence.** Previous work has studied the *dynamics* of learning (Saxe et al., 2014; Bordelon & Pehlevan, 2025; Proca et al., 2025), by approaches including *dynamical* mean-field theory (Bordelon & Pehlevan, 2022b), but comes at the cost of making simplifying assumptions (Saxe et al., 2014; Proca et al., 2025) or complicated expressions. We here join a line of recent work that

instead seeks out to only describe the network state after training when the weights have converged to a stationary distribution, significantly simplifying the theory (Seung et al., 1992; Cohen et al., 2021; Seroussi et al., 2023; Cui et al., 2023; Fischer et al., 2024; van Meegen & Sompolinsky, 2025; Lauditi et al., 2025).

### 3. Results

#### 3.1. Unified feature learning theory for RNNs and DNNs

We consider a general architecture with hidden dimension  $N$  and input dimension  $D$ . At each timestep  $t$ , the pre-activations  $\mathbf{h}^t \in \mathbb{R}^N$  receive external temporally-dependent input  $\mathbf{x}^{t-1} \in \mathbb{R}^D$  through read-in weights  $\mathbf{U} \in \mathbb{R}^{N \times D}$  and recurrent inputs  $\phi(\mathbf{h}^{t-1})$  through hidden weights  $\mathbf{W} \in \mathbb{R}^{N \times N}$ , where  $\phi(\circ)$  is an elementwise activation function. The scalar output of the architecture  $f^{t+1}$  is obtained through readout weights  $\mathbf{V} \in \mathbb{R}^{1 \times N}$ , so that the whole architecture reads

$$\begin{aligned} \mathbf{h}^t &= \mathbf{W}^{(t-1)} \phi(\mathbf{h}^{t-1}) + \mathbf{U} \mathbf{x}^{t-1}, \\ f^{t+1} &= \mathbf{V} \phi(\mathbf{h}^t), \end{aligned} \quad (1)$$

$$\mathbf{W}^{(t)} = \begin{cases} \mathbf{W}, & \text{RNN} \\ \mathbf{W}^{(t)}, & \text{DNN} \end{cases}$$

with  $t = 1, \dots, T-1$ . We will abbreviate this penultimate timestep with  $T_- := T-1$  from here on.

We group all parameters into  $\Theta$  and abbreviate  $\phi^t := \phi(\mathbf{h}^t)$ . Besides RNNs, this definition encompasses also DNNs, where  $\mathbf{x}^0$  is the input and  $f^T$  the output (see Section A.3 for details).

We optimize this model via gradient descent on a mean-squared loss  $\mathcal{L}(\Theta; y, \mathbf{x}) = \frac{1}{2} \frac{1}{P|\mathcal{T}|} \sum_p^P \sum_{t \in \mathcal{T}} (y_p^t - f_p^t(\Theta, \mathbf{x}))^2$  over samples  $p$  and supervised timesteps  $t \in \mathcal{T}$ . For each gradient update, we allow for an i.i.d. Gaussian noise of strength  $\sqrt{2K}$  and an independent weight decay of strength  $\frac{\kappa}{G_\theta}$ , so that the overall update reads

$$\theta_{s+1} = \theta_s - \nabla_{\theta} \mathcal{L}(\Theta_s) ds - \frac{\kappa}{G_\theta} \theta_s ds + \sqrt{2K} ds \xi_s. \quad (2)$$

This update is commonly referred to as SGLD (stochastic gradient Langevin dynamics) (Naveh et al., 2020). This can be thought of as a naive approximation of stochastic gradient descent (SGD), replacing mini-batch fluctuations by uncorrelated noise. It can be shown that after convergence this algorithm samples from a stationary distribution  $\theta \sim P(\Theta|y, \mathbf{x}) \propto \exp\{-P\mathcal{L}(\Theta; y, \mathbf{x})/\kappa - \frac{1}{2} \sum_\theta \|\theta\|^2/G_\theta\}$  (Gardiner, 1983; Seung et al., 1992; Kardar, 2007). This distribution can likewise be interpreted as a Bayesian posterior combining two factors: first, a base distribution that is a Gaussian i.i.d. weight prior  $P(\Theta) \propto \exp\{-\frac{1}{2} \sum_\theta \|\theta\|^2/G_\theta\} \propto \mathcal{N}(\Theta|0, G_\theta)$ , and a likelihood  $\propto \exp\{-P\mathcal{L}(\Theta; y, \mathbf{x})/\kappa\}$ , which may alternatively

be regarded as a Bayesian regularization due to noisy labels,  $y_p^t = f_p^t + \sqrt{K} \xi_p^t$ .

We show in Section A.3 that it is possible to translate “structure to function” by marginalizing out the prior weights  $\Theta$  in favor of a distribution that only depends on neural activations  $h$ , input  $\mathbf{x}$ , and labels  $y$ :

$$P(h|y, \mathbf{x}) \propto \exp \left\{ -\frac{1}{2} \text{tr} [\mathbb{Y}_\mathcal{T} (v \Phi_\mathcal{T}^- + \kappa)^{-1} \right. \\ \left. - \frac{1}{2} \mathbf{h}^\top (w [\Phi^-] + u \mathbb{X}^-)^{-1} \mathbf{h} + \phi(\mathbf{h})^\top \tilde{C} \phi(\mathbf{h}) \right\}. \quad (3)$$

In making this change, this theory summarizes the effect of weight learning in the form of a *kernel*

$$\Phi_{pp}^{tt'} := \frac{1}{N} \sum_i^N \phi(h_{i,p}^t) \phi(h_{i,p'}^{t'}) \quad (4)$$

$$\stackrel{N \rightarrow \infty}{\asymp} \langle \phi(h_p^t) \phi(h_p^{t'}) \rangle_{P(h|y, \mathbf{x})}. \quad (5)$$

In these expressions, contractions  $a^\top b := \sum_p^P \sum_t^T a_p^t b_p^t$  are taken over the joint pattern-time space, and  $(\circ^-)^{tt'} := \circ^{t-1, t'-1}$  is a shorthand to indicate time-shift. Likewise,  $\mathbb{X}_{pp'}^{tt'} := \frac{1}{D} \sum_i^D x_{p,i}^t x_{p',i}^{t'}$  and  $\mathbb{Y}_{pp'}^{tt'} := y_p^t y_{p'}^{t'}$  denote input and label kernels, and  $\mathbb{H}_{pp'}^{tt'} := \frac{1}{N} \sum_i^N h_{p,i}^t h_{p',i}^{t'} \asymp \langle h_p^t h_{p'}^{t'} \rangle_{P(h|y, \mathbf{x})}$  is the kernel for the preactivations, defined in analogy to the kernel  $\Phi$  for the postactivations in (4). A subscript  $\circ_\mathcal{T}$  denotes the restriction of a kernel to the supervised timesteps  $\mathcal{T}$ , and  $\Phi, \mathbb{H}$ , and  $\tilde{C}$  are matrices in  $\mathbb{R}^{PT_- \times PT_-}$ . In this theory, RNNs and DNNs only differ by a *masking operation* in time,  $[\Phi^-] := \begin{cases} \Phi^-, & \text{RNN} \\ \text{diag}(\Phi^-), & \text{DNN} \end{cases}$ , capturing the effect of the DNN’s weight independence in form of the correlation of the  $h$ -fields across timesteps. We discuss the effect of this difference in the following sections.

As we show in Section A.3 in the large  $N$  limit, the empirical averages  $\frac{1}{N} \sum_i^N$  concentrate to a well-defined value. The conjugate variable  $\tilde{C}(\mathbb{H}, \Phi) = \tilde{C}_y + \tilde{C}_h$  encodes the two constraints that the activity  $h$  is subjected to:  $\tilde{C}_y = \frac{1}{2} v (v \Phi^- + \kappa)^{-1} \mathbb{Y} (v \Phi^- + \kappa)^{-1}$  aligns the representation towards the targets  $y^t$ , whereas  $\tilde{C}_h = \frac{1}{2} w (w [\Phi^-] + u \mathbb{X}^-)^{-1} (\mathbb{H} - (w [\Phi^-] + u \mathbb{X}^-)) (w [\Phi^-] + u \mathbb{X}^-)^{-1}$  acts as a force on  $\phi(h)$  towards the prior describing the forward pass  $\mathbf{h}^t = \mathbf{W}^{(t-1)} \phi^{t-1} + \mathbf{U} \mathbf{x}^{t-1}$  with untrained weights. The scalars  $u, w, v$  are intensive parameters that reparametrize the scales of the weights  $G_\theta$  so that the kernels become intensive (i.e.,  $\mathcal{O}(1)$  with respect to  $N$ ) quantities that concentrate, and we likewise reparametrized  $K$  by the intensive quantity  $\kappa$  (see Section A.3). In the limit of large networks, the replacement of the empirical average over neuron indices (4) with an average that factorizes over neurons (5) becomes exact; that is, the empirical average is

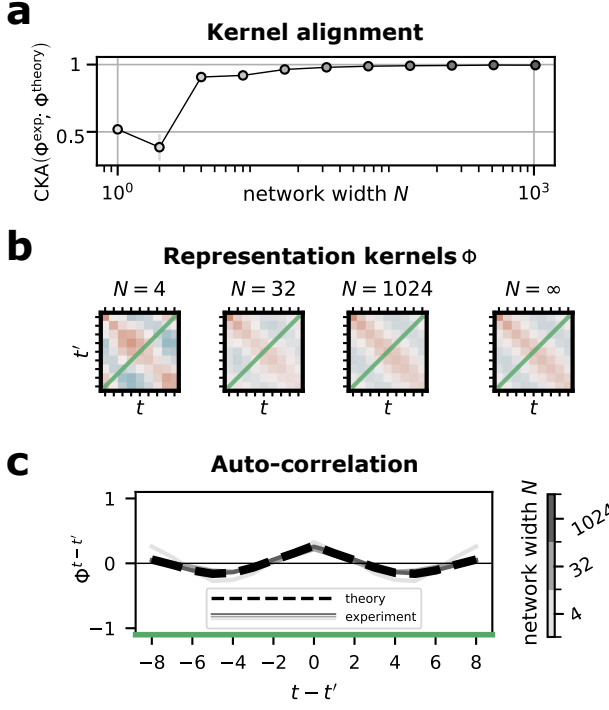


**Figure 2. Kernels in trained RNNs converge to theory predictions for large network width  $N$ .** We train an RNN as described in (2) with nonlinear activation function  $\phi(\circ) = \text{erf}(\frac{\sqrt{2}}{2}\circ)$  to produce a sinusoidal target sequence  $y^t = \cos(\frac{2\pi}{T}t)$ ,  $T = 10$  in response to a scalar input at time  $t = 0$ , i.e.  $x^t = \delta^{t_0}$ . **a**) Centered kernel alignment (CKA) between the kernel  $\Phi_{\text{exp.}}(\Theta) = \frac{1}{N} \sum_i^N \phi(h_i)\phi(h_i)^\top$  from explicit weight SGLD experiments at different network widths  $N$  and the kernel  $\Phi_{\text{theory}} = \langle \phi(h)\phi(h)^\top \rangle_{P(h|y, \mathbf{x})}$  predicted by the theory (5) for  $N \rightarrow \infty$ . **b**) Temporal structure of kernels  $\Phi_{\text{exp.}}$  for different finite network widths compared to  $\Phi_{\text{theory}}$  at infinite width  $N \rightarrow \infty$ . **c**) Autocorrelation function of the network measured along the anti-diagonal  $\Phi^{t-t'}$  of the kernel (dashed: theory; full curve: numerics), marked in green in panel **b**.

self-averaging due to concentration.

In deriving (3), we traded the posterior distribution  $P(\Theta|y, \mathbf{x})$  over parameters of extensive size in  $N$  for a distribution  $P(h|y, \mathbf{x}) = P(h|\Phi, \tilde{C}, \mathbb{Y}, \mathbb{X})$  over a single variable  $h_i \equiv h$  which is identically distributed over neurons, and only depends on the kernels  $\Phi, \tilde{C}, \mathbb{Y}, \mathbb{X}$ . This theory straightforwardly recovers the  $\mu\mathbf{P}$  scaling (Yang & Hu, 2020) for the prior variances as  $(G_U, G_W, G_V) = (u/D, w/N, v/N^2)$  as well as  $\mathbf{K} = \kappa/N$ , from two requirements: that pre-activations  $h$  scale suitably in the  $N \rightarrow \infty$  limit (in particular avoiding exploding/vanishing gradients), and permitting feature learning in terms of a change to the representation kernel  $\Phi$ . Moreover, the theory will allow us to directly characterize representational and functional properties of the networks, which will be our focus in the following. We first test whether the theory can accurately capture the effects of

weight sharing via a simple time-series regression task in Fig. 2 before we leverage it in the following sections to explain consequences of weight sharing. To this end, we compare kernels  $\Phi_{\text{exp.}}^{tt'}(\Theta) = \frac{1}{N} \sum_i^N \phi(h_i^t)\phi(h_i^{t'})$  measured from networks trained through SGLD experiments in weight space, and kernels  $\Phi_{\text{theory}}^{tt'} = \langle \phi(h^t)\phi(h^{t'}) \rangle_{P(h|y, \mathbf{x})}$  predicted by the theory (3). We use centered kernel alignment  $\text{CKA}(\Phi_{\text{exp.}}(\Theta), \Phi_{\text{theory}})$  (Cortes et al., 2012; Fischer et al., 2024), which computes the cosine similarity of the vectorized matrices after subtracting their means. In Fig. 2a, the alignment between theory and simulations increases with the network width  $N$  as expected, since the empirical average we defined in (4) converges with the number of constituting terms. Notably, we obtain an accurate description of the network kernels already at large but finite network width.

The trained networks exhibit a non-trivial temporal correlation structure, visible as non-diagonal kernels in Fig. 2b; the anti-diagonal yields the autocorrelation function shown in Fig. 2c, which likewise converges to the theoretical prediction for large  $N$ . In this setting, where there are no correlations in the input, there are potentially two contributions to the observed temporal coherence: the weight sharing over time and the temporal correlation in the supervision signal  $y$ . In the following sections, we use our theory to separate these contributions, showing that such temporal correlations are specific to RNNs due to weight sharing across timesteps, which is absent in feed-forward architectures. In Section 3.2, we focus on *endpoint-supervised* tasks that are the typical use case of DNNs, and in Section 3.3 we focus on *sequential* tasks that are the typical use case of RNNs.

### 3.2. Phase transition towards temporal coherence in RNNs induced by strong learning signal in endpoint-supervised tasks

The formulation in (1) allows us to draw a direct comparison to deep neural networks (DNNs) via unrolling RNNs in time with a one-to-one correspondence between RNN timesteps  $t$  and DNN layers, which we thus also index by  $t$ . DNNs are typically trained on tasks in which inputs are provided only at the first layer and supervision is applied only at the final layer; we hereafter refer to this setting as *endpoint-supervised*. Equation (1) for the DNN then becomes

$$\begin{aligned} \mathbf{h}^1 &= \mathbf{U}\mathbf{x}^0, \\ \mathbf{h}^t &= \mathbf{W}^{(t-1)}\phi(\mathbf{h}^{t-1}), \quad 2 \leq t < T, \\ \mathbf{f}^T &= \mathbf{V}\phi(\mathbf{h}^{T-1}). \end{aligned} \quad (6)$$

As we detail in Section A.3.4, DNNs can be understood as a special case of the general mean-field theory developed in Section 3.1 by omitting input at timesteps  $t > 1$ , and having no supervision target at timesteps  $t < T$ . Notably, DNNs

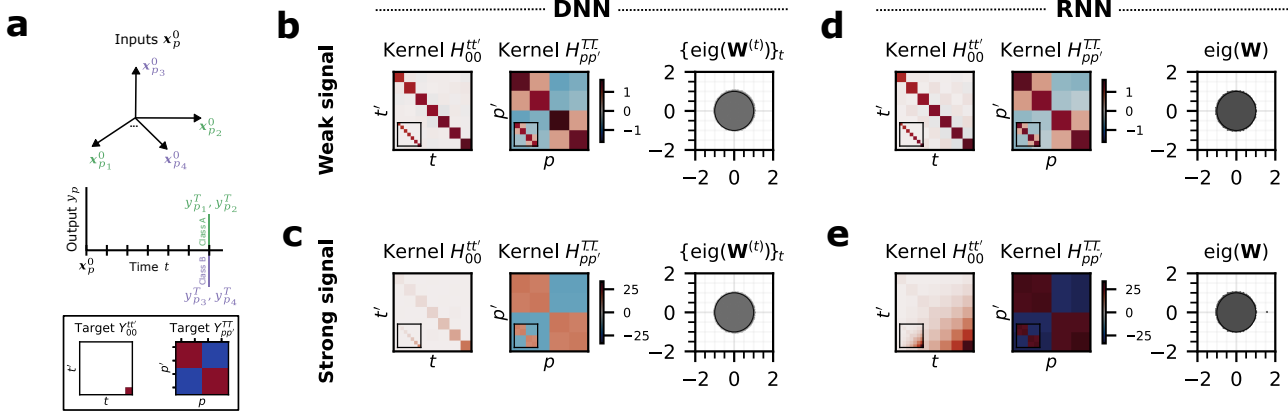


**Figure 3. RNNs and DNNs learn similar spatial representations while only RNNs learn temporal coherence for strong learning signal.** **a)** Binary classification task:  $P = 4$  pairwise orthogonal inputs  $\mathbf{x}_p \in \mathbb{R}^D$  with  $D = 4$  map to labels  $y_p \in \{-1, 1\}$ , as summarized by kernels  $\mathbb{Y}_{00}^{tt'} \in \mathbb{R}^{T_- \times T_-}$ ,  $\mathbb{Y}_{pp}^{TT} \in \mathbb{R}^{P \times P}$ . **b-e)** Kernel and weight structure of DNNs (panels **b**, **c**) and RNNs (panels **d**, **e**) trained on the task. Lower-left insets show prediction by the kernel theory. We consider the cases of weak (upper row) or strong learning signal (lower row). From left to right in each cell (panels **b-e**): temporal kernel  $\mathbb{H}_{00}^{tt'}$  for fixed pattern  $p = 0$ , sample kernel  $\mathbb{H}_{pp'}^{T_- T_-} := \frac{1}{N} \mathbf{h}_p^{T_-} \cdot \mathbf{h}_{p'}^{T_-}$  in last timestep  $T_- := T - 1 = 7$ , and eigenspectrum in the complex plane of hidden weights  $\mathbf{W}$  (RNN) or  $\{\mathbf{W}^{(t)}\}_t$  (DNN, eigenspectra of all  $\{\mathbf{W}^{(t)}\}_t$  plotted on same axis), with  $N = 2048$ . Other parameters:  $w = v = u = 1$ ,  $\kappa = 0.1$ .

in addition have independent weight priors  $\mathbf{W}^{(t)}$  across timesteps, reflected in a factorization of the prior introduced in Section 3.1,  $P_{\text{DNN}}(\{\mathbf{W}^{(t)}\}_t) = \prod_{t=1}^{T-1} P(\mathbf{W}^{(t)})$ .

Despite these similarities, it is unclear what is the effect that weight sharing in the RNN has on representation (i.e., the kernels  $\Phi, \mathbb{H}$ ) or on computation (i.e., the model output  $f$ ). Segadlo et al. (2022) show that in the NNGP limit (i.e., when non-readout weights don't change during training), temporal correlations in RNNs with point-symmetric activation functions vanish, and the kernel representations in DNNs and RNNs therefore coincide. Here, we generalize their theoretical approach to account for feature learning under  $\mu$ P scaling. Our theory reveals a distinction between the kernels in RNNs and DNNs in endpoint supervised tasks, but only if the learning signal is sufficiently strong (Fig. 3, here for simplicity for linear activation, i.e.  $\phi(h) \rightarrow h$ ,  $\Phi \rightarrow \mathbb{H}$ ). We find a qualitative change in the RNN's kernel representation from a *temporally incoherent* to a *temporally coherent* regime that is absent in DNNs. Here, temporally coherent means that the vectors  $\frac{1}{N} \mathbf{h}^t \cdot \mathbf{h}^{t'}$  between timesteps  $t$  and  $t'$  align. This change is accompanied by an outlier eigenvalue in the spectrum of  $\mathbf{W}$ . We find that this transition is controlled by the strength of the learning signal  $\lambda = y^2 / v w^{T-2} u$  relative to the  $\mathcal{O}(1)$  parameters  $u, w, v$  that define the scale of the weights, a dependence that we characterize more quantitatively below.

The pattern-by-pattern kernel  $\mathbb{H}_{pp'}^{T_- T_-}$  in the last time point  $T_- := T - 1$  determines the predictor statistics of the network via  $f^T = v \mathbb{H}_{pp'}^{T_- T_-} (v \mathbb{H}_{pp'}^{T_- T_-} + \kappa)^{-1} y^T$  (Neal, 1996; Jacot

et al., 2018). Interestingly, Fig. 3 reveals that the block structure induced by class membership is present in both RNNs and DNNs and differs only in scale, hence leading to qualitatively similar predictors. This reflects that both networks have learned the pattern-by-pattern structure  $\mathbb{Y}$  that defines the task (Fig. 3a), in particular the last timestep's representation  $\mathbb{H}_{pp'}^{T_- T_-} \simeq \mathbb{Y} = yy^T$  has learned  $y$  as an eigenvector (cf. Fischer et al. (2024)).

We now seek a theoretical understanding behind this phenomenon. For simplicity, we here consider only the linear case (we show in Section A.8 that the transition also persists in the non-linear case). From the theory (3) that yields the probability distribution of the preactivations, we obtain a probability over representations via  $P(\mathbb{H}|y, \mathbf{x}) = \langle \delta(\mathbb{H} - hh^T) \rangle_{P(h|\Phi, \tilde{C}, \mathbb{Y}, \mathbf{x})}$  after replacing  $\tilde{C} = \tilde{C}(\mathbb{H})$  by its stationarity condition (Section A.4):

$$-\ln P(\mathbb{H}|y, \mathbf{x})/N = \frac{1}{2} \text{tr} [\mathbb{Y}_T (v \mathbb{H}_T^- + \kappa)^{-1}] + \frac{1}{2} \text{tr} [\mathbb{H} (w [\mathbb{H}^-] + u \mathbb{X}^-)^{-1}] - \frac{1}{2} \ln \frac{|\mathbb{H}|}{|w [\mathbb{H}^-] + u \mathbb{X}^-|}, \quad (7)$$

where  $[\mathbb{H}^-] := \begin{cases} \mathbb{H}^-, & \text{RNN} \\ \text{diag}(\mathbb{H}^-), & \text{DNN} \end{cases}$  again is the architecture-dependent masking and  $|\circ|$  is the determinant. The second line takes the form of a Kullback-Leibler divergence  $D_{\text{KL}}(\mathcal{N}_h(\mathbb{H}) \parallel \mathcal{N}_h(w [\mathbb{H}^-] + u \mathbb{X}^-))$  that vanishes at the NNGP prior which describes the forward propagation under random weights. For the endpoint-supervised tasks we consider here, the first term has support only on the last

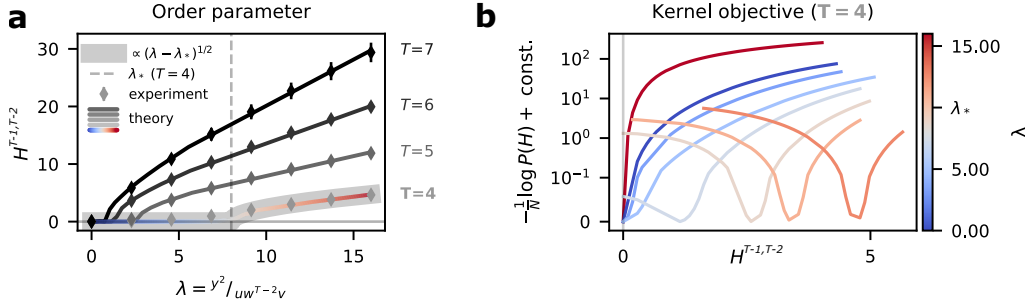


**Figure 4. Second-order phase transition in linear RNNs of  $T = 4$  with critical exponent  $\frac{1}{2}$ .** a) Off-diagonal kernel order parameter  $\mathbb{H}^{T-1,T-2}$  as a function of the control variable  $\lambda$ . Solid curves: kernel theory for different network depths. Diamonds: empirical kernel from weight SGLD. b) Negative log-probability for the off-diagonal order parameter  $\mathbb{H}^-$ , obtained from maximizing  $P(\mathbb{H}|\mathbb{H}^{T-1,T-2}, y, \mathbf{x})$  as a function of the signal strength control variable  $\lambda$ . Network width  $N = 2048$  (error bars: residual fluctuation at the equilibrium of the update (2)).

timestep,  $(v\mathbb{H}_T^- + \kappa)^{-1}\mathbb{Y}_T \rightarrow (v\mathbb{H}^{T-T_-} + \kappa)^{-1}\mathbb{Y}^{TT}$ .

**Temporally-incoherent regime** For small learning signal  $\lambda$ , the representation kernels  $\mathbb{H}$  of DNNs and RNNs coincide. The consistency of the diagonal solution with the saddle point equations for the RNN can be seen as follows: due to the masking operation in the DNN, a diagonal kernel is a stationary point. Inserting such a diagonal solution into the saddle point equations for the RNN, there are no terms that would cause off-diagonal correlations. The diagonal solution hence obeys the saddle point conditions of the RNN, too. What is unclear, though, is whether this is the only stationary point. The RNN could have additional solutions with non-vanishing off-diagonal elements that attain a higher likelihood than the diagonal solution. Indeed for larger  $\lambda$  this will be the case.

Since the output  $f$  after learning depends only on the kernel  $\mathbb{H}$ , in the temporally-incoherent regime, both DNNs and RNNs yield the same predictions and thus have the same generalization properties.

**Temporally-coherent regime** An explicit analytical form for the kernel  $\mathbb{H}$  can be derived for the minimal case of  $T = 4$  (details in Section A.5). As we show there, the continuous change in the order parameter is the signature of a second-order phase transition with a critical exponent  $\frac{1}{2}$ , where the kernel's off-diagonal  $\mathbb{H}^{T-1,T-2}$  forms the order parameter controlled by  $\lambda$ . Fig. 4 shows this transition for  $T = 4$  and for larger  $T$ . For the latter case, to the best of our knowledge, no explicit form is available. The transition prescribed by our mean-field theory is closely followed by the kernel measured from direct SGLD experiments on the weights  $\mathbf{U}, \mathbf{W}, \mathbf{V}$  (solid curves and diamonds, respectively, in Fig. 4a). The phase transition thus casts learning as an optimization problem, but with the weight loss  $\mathcal{L}(\Theta; y, \mathbf{x})$  replaced by a lower-dimensional objective over kernels,  $-\ln P(\mathbb{H}|y, \mathbf{x})/N$ , which is shown in Fig. 4.

Depending on the control parameter  $\lambda$ , this kernel objective has a unique minimum only at the temporally-incoherent solution when  $\lambda$  is small, but this minimum becomes unstable in favor of a new minimum at the coherent solution beyond the transition point (see Fig. 4b).

The analytics for  $T = 4$  developed in Fig. 4 for (7) suggest an energy-entropy tradeoff underlying this transition. In both architectures, the label likelihood in the first line increases the final variance  $\mathbb{H}^{T-T_-}$  by tying it to  $\mathbb{Y}^{TT}$  (“energy”, cf. (11)). However, this incurs a penalty on  $\mathbb{H}^-$  in  $D_{\text{KL}}(\mathcal{N}_h(\mathbb{H}) \parallel \mathcal{N}_h(w[\mathbb{H}^-] + u\mathbb{X}^-))$  that is the second line of (7), which encourages the kernels to follow the NNGP iteration over time. In the DNN case, the masking  $[\mathbb{H}^-] = \text{diag}(\mathbb{H}^-)$  discards off-diagonals, so introducing temporal correlations cannot reduce the  $D_{\text{KL}}$ . Thus, they remain suppressed by the  $\ln |\mathbb{H}|$  term (an “entropic” penalty, since it favors uncorrelated  $\mathbb{H}$ ). In the RNN however, the increase in  $\mathbb{H}^{T-T_-}$  can be compensated by  $[\mathbb{H}^-] = \mathbb{H}^-$  through the introduction of temporal correlations. As it turns out, the marginal cost of the entropic penalty from off-diagonals eventually drops below the  $D_{\text{KL}}$  cost, once the labels  $\mathbb{Y}$  are sufficiently large relative to the priors  $u, w, v$  that enter it. Thus, eventually a transition point controlled by their ratio  $\lambda$  is reached, separating the phases.

### 3.3. RNN's weight sharing inductive bias generalizes efficiently for sequential tasks

In Section 3.2, we considered endpoint-supervised tasks, identifying qualitative difference in the representation across timesteps. While the last timestep's representation  $\mathbb{H}^{T-T_-}$  exhibited quantitative differences in terms of its scale, its qualitative structure was preserved, entailing similar predictors  $f$ . Since such tasks do not read out from different timesteps and hence are unaffected by temporal correlations, this leaves the question how RNNs and DNNs differ for tasks with non-trivial temporal structure. To investigate this, we now consider sequential tasks  $x^t \mapsto y^t$ , where intuitively

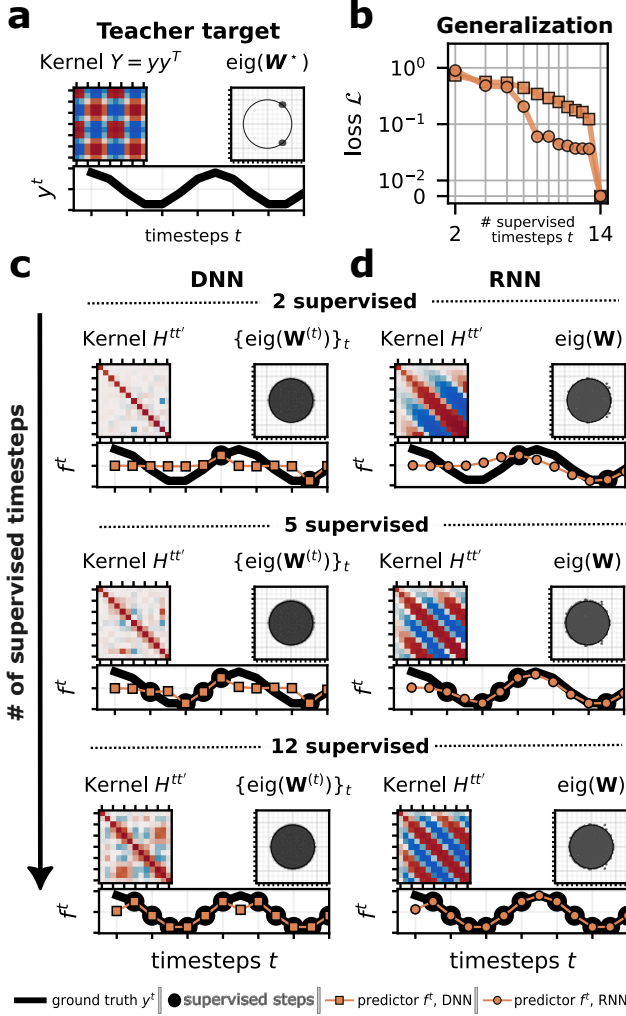


**Figure 5. RNNs have better sample efficiency in sequential tasks due to task-model alignment induced by weight sharing.** **a)** Sequence regression task, with supervision signal at variable numbers of timesteps  $t$ . Top left: Label kernel  $\mathbb{Y}$ . Top right: Spectrum of the teacher weights  $\mathbf{W}^*$ . Bottom: Sinusoidal output of the teacher. **b)** Generalization error  $\mathcal{L} = \frac{1}{2T} \sum_{t=2}^T (y^t - f^t)^2$  over all timesteps as a function of the number of supervised timesteps. **c-d)** Representation  $\mathbb{H}$  and output  $f^t$  underlying differences in generalization. DNN **(c)** and RNN **(d)** output for different number of supervision steps (rows). Each cell displays the time-by-time kernel for pattern  $p$  (top left), the weight eigenspectra ( $\{\mathbf{W}^{(t)}\}_t$  for DNN,  $\mathbf{W}$  for RNN; top right), and on the bottom a comparison of the target function  $y^t$  (black line) versus the network prediction  $f^t$  (orange) across supervised timepoints (black markers).

the RNNs' weight sharing may benefit generalization.

We consider a minimal setting where we have access to the ground truth learning signal  $y^t = x_0^0 \sin(\omega t) + x_1^0 \cos(\omega t)$  for  $\mathbf{x}^0 = [\cos(\varphi_0), \sin(\varphi_0)]^\top \in \mathbb{R}^{D=2}$ , with a single input pattern ( $P = 1$ ). Notably, this task is identical to a teacher RNN via  $y^t = \mathbf{V}^* (\mathbf{W}^*)^t \mathbf{U}^* \mathbf{x}^0$ , with aligned readin  $\mathbf{U}^* = \begin{bmatrix} 1 & 0 \\ 0 & 1 \end{bmatrix}$ , readout  $\mathbf{V}^* = \begin{bmatrix} 1 \\ 0 \end{bmatrix}$ , and recurrent  $\mathbf{W}^* = \begin{bmatrix} \cos(\Delta\varphi) & -\sin(\Delta\varphi) \\ \sin(\Delta\varphi) & \cos(\Delta\varphi) \end{bmatrix}$  weights. The teacher RNN dynamics thus describe a rotation of the input vector  $\mathbf{x}^0$  in a 2D plane by an angle  $\Delta\varphi$  in each timestep. In Fig. 5, we find that RNNs trained on this task learn structured sequences from fewer samples (since  $P = 1$ , the number of supervised timesteps takes the role of a sample count). From a Bayesian perspective, the reason for this difference is the learned change in the kernel due to the masking operation  $\llbracket \dots \rrbracket$  in (3), which in turn determines the predictor via  $f^t = \sum_{t' t''} \mathbb{H}^{t t'} ((\mathbb{H} + \kappa)^{-1})^{t'' t''} y^{t''}$ , where summations now go over timesteps. In the DNN, the posterior covariance  $\text{diag}(\mathbb{H})$  will always produce an incoherent representation  $h^t$  outside of the supervised training points, even after learning. This means that generalization effectively becomes Bayesian inference with an uncorrelated kernel, and thus extrapolating with the prior mean,  $f^t = 0$ . In contrast, the RNN's representation can develop correlations in  $h^t$  that match the target kernel  $\mathbb{Y}$  already after a few samples. In contrast to the DNN, this is accompanied by the recovery of the conjugate pair of teachers in the eigenvalues of  $\mathbf{W}$ , pointing to a structured change in the spectrum. This difference in generalization is perhaps surprising, since due to its weight sharing, the RNN's expressivity is a subset of that of a DNN.

While this argument showcases that temporal correlations in  $\mathbb{H}$  can develop, it remains unclear what is the mechanism that shapes them such that they indeed facilitate generalization. To understand this, we consider the kernel theory  $P(\mathbb{H}|\mathbb{Y}, \mathbb{X})$  in (7) for the linear case and pursue a perturbative expansion in the label strength  $\mathbb{Y}$ . Starting from the closed-form saddle-point equation for the learned kernels (see (8), (34)), we expand around the diagonal NNGP kernel  $\mathbb{H}_0$  (the solution in absence of feature learning) by writing  $\mathbb{H} = \mathbb{H}_0 + \Delta$ , with  $\Delta = \Delta_1 + \Delta_2 + \mathcal{O}(\mathbb{Y}^3)$ . The linear response  $\Delta_1$  turns out to not involve strong architectural effects, since masking  $\llbracket \mathbb{H}_0 \rrbracket$  is an identity operation on diagonal kernels. We consider then the second order  $\Delta_2$  to identify architecture-dependent effects. Introducing the NNGP observation covariance  $\mathbb{G}_y := (v\mathbb{H}_0 + \kappa)^{-1}$ , the leading correction can be written as

$$\begin{aligned} \mathbb{H} - \mathbb{H}_0 \approx & +\mathbb{G}_y \mathbb{Y}^+ \mathbb{G}_y \\ & - \left( {}^{w^2} \mathbb{H}_0^{-1} \llbracket \Delta_1 \rrbracket \mathbb{H}_0^{-1} \Delta_1 \mathbb{H}_0^{-1} + (\sim)^\top \right) + \dots \end{aligned} \quad \left. \right\} = \Delta_1 \quad (8)$$

where  $\llbracket \dots \rrbracket$  again is the identity for RNNs and a diagonal projection for DNNs,  $\mathbb{Y}^+$  denotes time shift,  $(\sim)^\top$  is the transpose of preceding term, and we omitted terms independent of masking “...” or that are of higher order  $\mathcal{O}(\mathbb{Y}^3)$ .

To interpret this expression, consider a time-diagonal  $\mathbb{X}$  and a kernel  $\mathbb{H}_0$  (Segadlo et al., 2022) with *constant* diagonal, conditions which are both met for Fig. 5 for  $u = w = v = 1$ . Then,  $\mathbb{H}_0^+$  is diagonal with entries  $\mathbb{h}_0^t$  and we may write  $\Delta_1 = \mathbb{G}_y \mathbb{Y}^+ \mathbb{G}_y \propto \mathbb{Y}^+$ .

In a DNN,  $\llbracket \Delta_1 \rrbracket = \text{diag}(\Delta_1)$  and the quadratic term acts entry-wise,

$$\Delta_{2,\text{DNN}}^{tt'} = -\frac{1}{\mathbb{h}_0^t} \left( \frac{1}{\mathbb{h}_0^t} \mathbb{Y}^{+tt} + \frac{1}{\mathbb{h}_0^{t'}} \mathbb{Y}^{+t't'} \right) \mathbb{Y}^{+tt'} \frac{1}{\mathbb{h}_0^{t'}} + \dots, \quad (9)$$

In an RNN, in contrast, we get

$$\Delta_{2,\text{RNN}}^{tt'} = -2 \frac{1}{\mathbb{h}_0^t} \left( \sum_{t''} \mathbb{Y}^{+tt''} \frac{1}{\mathbb{h}_0^{t''}} \mathbb{Y}^{+t''t'} \right) \frac{1}{\mathbb{h}_0^{t'}} + \dots. \quad (10)$$

This equation shows that the inverses appearing in (8) take the role of *propagators*, and hence (10) implements an interpolation between supervised points of  $\mathbb{Y}$ . To see this explicitly, consider the case that  $t_1$  and  $t_2$  have been observed but  $t_3$  has not. Then, the correlation  $\Delta_{2,\text{RNN}}^{t_3t_1}$  will interpolate across the path  $t_3 \leftarrow t_2 \leftarrow t_1$  that appears in the sum at  $t' = t_2$ , but  $\Delta_{2,\text{DNN}}^{t_3t_1} = 0$  in (9), making the posterior over  $h$  uncorrelated.

A complementary way to understand this is that  $\Delta_1$  is an  $\mathbb{H}_0$ -whitened version of  $\mathbb{Y}^+$ , and due to  $\mathbb{H}_0$ ’s diagonal structure will approximately inherit its eigenvectors. For the DNN, the masking in the second-order iteration (9) will destroy this structure, so that learning requires more samples.

In summary, this shows that the mechanism behind the inductive bias of weight sharing can be traced back to the propagation of label messages across unsupervised time points.

## 4. Discussion

**Summary.** In this work, we developed a unified theory of feature learning for RNNs and DNNs in terms of representational similarity kernels  $\Phi = \frac{1}{N} \sum_i^N \phi(h_i) \phi(h_i)^\top$  and  $\mathbb{H} = \frac{1}{N} \sum_i^N h_i h_i^\top$ , describing trained networks in the feature learning ( $\mu\text{P}$ ) regime. This theory reveals the functional implications of architectural structure: it describes how the representational kernels  $\Phi$  and  $\mathbb{H}$  as well as the predictor  $f$  are shaped by weight scales  $u, w, v$ , the structure of input  $\mathbb{X}$  and labels  $\mathbb{Y}$ , and the network architecture itself. In this theory, the key architectural difference between RNNs and DNNs, weight sharing across timesteps (layers), becomes a masking operation  $\llbracket \Phi \rrbracket$  on the temporal correlations of hidden activities  $\phi(h)$  in Equation (3), affecting the activities  $h$  and the predictor  $f$ .

**Phases of feature learning.** Feature learning is often characterized in terms of  $\mathcal{O}(1)$  changes in the representation (Yang & Hu, 2020; Bordelon & Pehlevan, 2022a). We find that, within this regime, a sufficiently strong learning signal  $\lambda$  is necessary in addition to drive *structured* alignment in RNNs: not merely changes in eigenvalues of the representational kernel, but alignment of its eigenvectors to the task covariance. This suggests a more granular view of feature learning beyond uniform changes in scale (Canatar et al., 2021; Li & Sompolsky, 2021): the learned eigenvectors themselves constitute the features that improve generalization, consistent with how the term “feature” is used in neuroscience (Hubel & Wiesel, 1962; Yamins et al., 2013). The phase transition we identify is reminiscent of a Baik-Ben Arous-Péché (BBP) transition (Baik et al., 2004), where random initialization acts as noise that gradient signals must overcome, mirroring similar findings by Bordelon & Pehlevan (2025).

**Connection to initialization.** In practice, feature learning is often controlled via initialization scale, small initialization leading to stronger representation of data features in the network learned. In our theory, the parameters  $u, w, v$  control a Gaussian prior over weights, and a narrow prior (large  $\lambda = y^2/uw^{T-2}v$ ) drives the representation from *temporally incoherent* to *temporally coherent*. These two perspectives match in the small noise regime  $\kappa \ll 1$ , where the diffusion over the Gaussian prior becomes much slower than changes due to the loss. Our theory thus details why small initialization aids feature learning.

**Inductive bias and task-model alignment.** A central finding is that weight sharing endows RNNs with an inductive bias that can outweigh the DNN’s greater expressivity. In sequential tasks, RNNs generalize from fewer samples due to a representation which infers the task structure, whereas DNNs effectively revert to a white prior outside supervised timesteps. This is in line with “No Free Lunch” theorems (Wolpert, 1996): the larger parameter count of DNNs need not be universally better when the inductive bias of a more constrained model matches the task structure. Our theory provides a mechanism behind this phenomenon in terms of interpolation between labels.

**Limitations and future work.** Regarding scope, our theory deliberately chooses a functional perspective by marginalizing over the weights, thereby abstracting away their learning dynamics and structure. Regarding training, we approximated the correlated mini-batch noise in plain SGD with independent noise of SGLD (Welling & Teh, 2011). Regarding tasks, we considered minimal settings to identify foundational mechanisms of learning via interpretable analytics; notably linear networks and orthogonal inputs. This choice has allowed us to focus on temporal generalization. However, there are important other phenomena in deep learning

that depend on the structure over patterns  $p$  (Sclocchi et al., 2024) or their interaction with timesteps  $t$ , particularly in proportional limits like  $T, P \propto N$ . Likewise, representations will be shaped by the cumulative application of nonlinearities across layers (Keup & Helias, 2022). While in principle our theory describes these cases as well, they go beyond the scope of this work.

## Acknowledgements

We would like to thank Alexander van Meegen and Antonio Sclocchi for helpful discussions. This work is supported by the Gatsby Charitable Foundation (GAT3850 to JPB and AP), and the Simons Foundation (1156607 to AP) and by the Deutsche Forschungsgemeinschaft (DFG, German Research Foundation) - 368482240/GRK2416, the Helmholtz Association Initiative and Networking Fund under project number SO-092 (Advanced Computing Architectures, ACA), the Deutsche Forschungsgemeinschaft (DFG, German Research Foundation) as part of the SPP 2205 – 533396241, and the DFG grant 561027837/HE 9032/4-1 (to MH).

## Impact statement

This paper presents work whose goal is to advance the field of Machine Learning. There are many potential societal consequences of our work, none which we feel must be specifically highlighted here.

## References

Aiudi, R., Pacelli, R., Baglioni, P., Vezzani, A., Burioni, R., and Rotondo, P. Local kernel renormalization as a mechanism for feature learning in overparametrized convolutional neural networks. *Nature Communications*, 16(1):568, January 2025. ISSN 2041-1723. doi: 10.1038/s41467-024-55229-3.

Alemohammad, S., Wang, Z., Balestiero, R., and Baraniuk, R. The Recurrent Neural Tangent Kernel, June 2021.

Amari, S.-I. Characteristics of random nets of analog neuron-like elements. *SMC-2(5):643–657*, 1972. ISSN 2168-2909. doi: 10.1109/TSMC.1972.4309193.

Ariosto, S., Pacelli, R., Pastore, M., Ginelli, F., Gherardi, M., and Rotondo, P. Statistical mechanics of deep learning beyond the infinite-width limit. 2023.

Atanasov, A., Bordelon, B., and Pehlevan, C. Neural Networks as Kernel Learners: The Silent Alignment Effect. *ArXiv*, October 2021.

Baik, J., Arous, G. B., and Peche, S. Phase transition of the largest eigenvalue for non-null complex sample covariance matrices, October 2004.

Besag, J. Comments on “Representations of knowledge in complex systems” by U. Grenander and M. I. Miller. *Journal of the Royal Statistical Society, Series B*, 56:591–592, 1994.

Bordelon, B. and Pehlevan, C. Population codes enable learning from few examples by shaping inductive bias. *bioRxiv : the preprint server for biology*, pp. 2021–03, 2022a.

Bordelon, B. and Pehlevan, C. Self-Consistent Dynamical Field Theory of Kernel Evolution in Wide Neural Networks, October 2022b.

Bordelon, B. and Pehlevan, C. Deep Linear Network Training Dynamics from Random Initialization: Data, Width, Depth, and Hyperparameter Transfer, February 2025.

Bordelon, B., Zavatone-Veth, Jacob, and Pehlevan, Cengiz. Mean-field theory of representation learning in RNNs. In *Abstracts and Posters*, Lisbon, 2024.

Canatar, A., Bordelon, B., and Pehlevan, C. Spectral Bias and Task-Model Alignment Explain Generalization in Kernel Regression and Infinitely Wide Neural Networks. *Nature Communications*, 12(1):2914, December 2021. ISSN 2041-1723. doi: 10.1038/s41467-021-23103-1.

Cohen, O., Malka, O., and Ringel, Z. Learning curves for overparametrized deep neural networks: A field theory perspective. 3:023034,

2021. doi: 10.1103/PhysRevResearch.3.023034. URL <https://link.aps.org/doi/10.1103/PhysRevResearch.3.023034>.

Cortes, C., Mohri, M., and Rostamizadeh, A. Algorithms for learning kernels based on centered alignment. 13(28): 795–828, 2012. URL <http://jmlr.org/papers/v13/cortes12a.html>.

Cui, H., Krzakala, F., and Zdeborova, L. Bayes-optimal learning of deep random networks of extensive-width. In *Proceedings of the 40th International Conference on Machine Learning*, volume 202, pp. 6468–6521. PMLR, 23–29 Jul 2023. URL <https://proceedings.mlr.press/v202/cui23b.html>.

Fischer, K., Lindner, J., Dahmen, D., Ringel, Z., Krämer, M., and Helias, M. Critical feature learning in deep neural networks, 2024.

Gardiner, C. W. *Handbook of Stochastic Methods for Physics, Chemistry and the Natural Sciences*. Number 13 in Springer Series in Synergetics. Springer-Verlag, Berlin, 1983.

Gardiner, C. W. *Handbook of Stochastic Methods for Physics, Chemistry and the Natural Sciences*. Number 13 in Springer Series in Synergetics. Springer-Verlag, Berlin, 2nd edition, 1985. ISBN 3-540-61634-9, 3-540-15607-0.

Hubel, D. H. and Wiesel, T. N. Receptive fields, binocular interaction, and functional architecture in the cat's visual cortex. 160:106–154, 1962.

Jacot, A., Gabriel, F., and Hongler, C. Neural tangent kernel: Convergence and generalization in neural networks. In *Advances in Neural Information Processing Systems 31*, pp. 8580–8589, 2018. URL <https://proceedings.neurips.cc/paper/2018/file/5a4be1fa34e62bb8a6ec6b91d2462f5a-Paper.pdf>.

Kadmon, J. and Sompolinsky, H. Transition to chaos in random neuronal networks. *Physical Review X*, 5(4): 041030, 2015.

Kalman, R. E. A new approach to linear filtering and prediction problems. 1960.

Kardar, M. *Statistical Physics of Particles*. Cambridge University Press, Cambridge, England, 2007.

Keup, C. and Helias, M. Origami in N dimensions: How feed-forward networks manufacture linear separability. 2022. doi: 10.48550/arXiv.2203.11355.

Kunin, D., Raventós, A., Dominé, C., Chen, F., Klindt, D., Saxe, A., and Ganguli, S. Get rich quick: Exact solutions reveal how unbalanced initializations promote rapid feature learning, October 2024.

Landau, I. D. and Sompolinsky, H. Coherent chaos in a recurrent neural network with structured connectivity. 14(12):e1006309, 2018. doi: 10.1371/journal.pcbi.1006309.

Lauditi, C., Bordelon, B., and Pehlevan, C. Adaptive kernel predictors from feature-learning infinite limits of neural networks, February 2025.

Lee, J., Sohl-Dickstein, J., Pennington, J., Novak, R., Schoenholz, S., and Bahri, Y. Deep neural networks as gaussian processes. In *International Conference on Learning Representations*, Vancouver, 2018. Open-Review.net. URL <https://openreview.net/forum?id=B1EA-M-0Z>.

Li, Q. and Sompolinsky, H. Statistical Mechanics of Deep Linear Neural Networks: The Back-propagating Kernel Renormalization. 11(3): 031059, 2021. doi: 10.1103/PhysRevX.11.031059. URL <https://journals.aps.org/prx/abstract/10.1103/PhysRevX.11.031059>.

Mastrogiuseppe, F. and Ostojic, S. Intrinsically-generated fluctuating activity in excitatory-inhibitory networks. 13(4):e1005498, 2017.

Mastrogiuseppe, F. and Ostojic, S. A Geometrical Analysis of Global Stability in Trained Feedback Networks. 31(6):1139–1182, 06 2019. ISSN 0899-7667. doi: 10.1162/neco\_a\_01187. URL [https://doi.org/10.1162/neco\\_a\\_01187](https://doi.org/10.1162/neco_a_01187).

Molgedey, L., Schuchhardt, J., and Schuster, H. G. Suppressing chaos in neural networks by noise. *Physical review letters*, 69(26):3717, 1992.

Naveh, G., Ben-David, O., Sompolinsky, H., and Ringel, Z. Predicting the outputs of finite networks trained with noisy gradients. 2020.

Neal, R. M. *Bayesian Learning for Neural Networks*. Springer New York, 1996. doi: 10.1007/978-1-4612-0745-0. URL <https://doi.org/10.1007/978-1-4612-0745-0>.

Nguyen, T., Miller, K. D., and Palmigiano, A. Theory of interaction between untuned modulatory inputs and tuned sensory inputs. *bioRxiv : the preprint server for biology*, pp. 2025–04, 2025.

Pacelli, R., Ariosto, S., Pastore, M., Ginelli, F., Gherardi, M., and Rotondo, P. A statistical mechanics framework

for Bayesian deep neural networks beyond the infinite-width limit. *Nature Machine Intelligence*, 5(12):1497–1507, December 2023. ISSN 2522-5839. doi: 10.1038/s42256-023-00767-6.

Palmigiano, A., Fumarola, F., Mossing, D. P., Kraynyukova, N., Adesnik, H., and Miller, K. D. Common rules underlying optogenetic and behavioral modulation of responses in multi-cell-type V1 circuits. *bioRxiv : the preprint server for biology*, pp. 1–59, 2023.

Pereira-Obilinovic, U., Aljadeff, J., and Brunel, N. Forgetting leads to chaos in attractor networks. *Physical Review X*, 13(1):011009, 2023.

Proca, A. M., Dominé, C. C. J., Shanahan, M., and Mediáno, P. A. Learning dynamics in linear recurrent neural networks. In *Forty-Second International Conference on Machine Learning*, 2025.

Risken, H. *The Fokker-Planck Equation*. Springer Verlag Berlin Heidelberg, 1996. doi: 10.1007/978-3-642-61544-3\_4. URL [https://doi.org/10.1007/978-3-642-61544-3\\_4](https://doi.org/10.1007/978-3-642-61544-3_4).

Rubin, N., Fischer, K., Lindner, J., Dahmen, D., Seroussi, I., Ringel, Z., Krämer, M., and Helias, M. From Kernels to Features: A Multi-Scale Adaptive Theory of Feature Learning, February 2025.

Sanzeni, A., Palmigiano, A., Nguyen, T. H., Luo, J., Nassi, J. J., Reynolds, J. H., Histed, M. H., Miller, K. D., and Brunel, N. Mechanisms underlying reshuffling of visual responses by optogenetic stimulation in mice and monkeys. *Neuron*, 111(24):4102–4115.e9, December 2023. ISSN 08966273. doi: 10.1016/j.neuron.2023.09.018.

Saxe, A., McClelland, J., and Ganguli, S. Exact solutions to the nonlinear dynamics of learning in deep linear neural networks. In *International Conference on Learning Representations*, 2014.

Saxe, A. M., McClelland, J. L., and Ganguli, S. Exact solutions to the nonlinear dynamics of learning in deep linear neural networks. *arXiv preprint arXiv:1312.6120*, 2013.

Schuecker, J., Goedeke, S., and Helias, M. Optimal sequence memory in driven random networks. 8: 041029, 2018. doi: 10.1103/PhysRevX.8.041029. URL <https://link.aps.org/doi/10.1103/PhysRevX.8.041029>.

Schuessler, F., Mastrogiuseppe, F., Ostojic, S., and Barak, O. Aligned and oblique dynamics in recurrent neural networks. *eLife*, 13:RP93060, 2024.

Sclocchi, A., Favero, A., and Wyart, M. A Phase Transition in Diffusion Models Reveals the Hierarchical Nature of Data, December 2024.

Segadlo, K., Epping, B., van Meegen, A., Dahmen, D., Krämer, M., and Helias, M. Unified field theoretical approach to deep and recurrent neuronal networks. 2022. accepted.

Seroussi, I. and Ringel, Z. Separation of scales and a thermodynamic description of feature learning in some CNNs. *arXiv preprint arXiv:2112.15383*, 2021.

Seroussi, I., Naveh, G., and Ringel, Z. Separation of scales and a thermodynamic description of feature learning in some cnns. 14(1):908, 2023. URL <https://doi.org/10.1038/s41467-023-36361-y>.

Seung, H. S., Sompolinsky, H., and Tishby, N. Statistical mechanics of learning from examples. *Physical review A*, 45(8):6056, 1992.

Simon, J. B., Dickens, M., Karkada, D., and Deweese, M. The eigenlearning framework: A conservation law perspective on kernel ridge regression and wide neural networks. 2023.

Sompolinsky, H., Crisanti, A., and Sommers, H.-J. Chaos in random neural networks. *Physical review letters*, 61 (3):259, 1988.

Toyoizumi, T. and Abbott, L. F. Beyond the edge of chaos: Amplification and temporal integration by recurrent networks in the chaotic regime. 84(5):051908, 2011a.

Toyoizumi, T. and Abbott, LF. Beyond the edge of chaos: Amplification and temporal integration by recurrent networks in the chaotic regime. *Physical Review E*, 84(5): 051908, 2011b.

Tu, Z., Aranguri, S., and Jacot, A. Mixed Dynamics In Linear Networks: Unifying the Lazy and Active Regimes. 2024.

van Meegen, A. and Sompolinsky, H. Coding schemes in neural networks learning classification tasks. *Nature Communications*, 16(1):3354, April 2025. ISSN 2041-1723. doi: 10.1038/s41467-025-58276-6.

Welling, M. and Teh, Y. W. Bayesian learning via stochastic gradient Langevin dynamics. In *Proceedings of the 28th International Conference on Machine Learning (ICML-11)*, pp. 681–688, 2011.

Wolpert, D. H. The lack of a priori distinctions between learning algorithms. *Neural computation*, 8(7):1341–1390, 1996.

Yamins, D. L., Hong, H., Cadieu, C., and DiCarlo, J. J. Hierarchical modular optimization of convolutional networks achieves representations similar to macaque it and human ventral stream. In Burges, C., Bottou, L., Welling, M., Ghahramani, Z., and Weinberger, K. (eds.), Advances in Neural Information Processing Systems, volume 26. Curran Associates, Inc., 2013. URL [https://proceedings.neurips.cc/paper\\_files/paper/2013/file/9a1756fd0c741126d7bbd4b692ccbd91-Paper.pdf](https://proceedings.neurips.cc/paper_files/paper/2013/file/9a1756fd0c741126d7bbd4b692ccbd91-Paper.pdf).

Yang, G. and Hu, E. J. Feature Learning in Infinite-Width Neural Networks. 2020. URL <https://arxiv.org/abs/2011.14522>.

Zavatone-Veth, J. A. and Pehlevan, C. Exact marginal prior distributions of finite bayesian neural networks. virtual, 2021. NeurIPS 2021. URL <https://openreview.net/forum?id=MxE7xFzv0N8>.

## A. Appendix

### Overview

We structure the Appendix as follows: we first in [Section A.1](#) establish the connection between Bayesian inference and the stationary distribution of stochastic gradient Langevin dynamics (SGLD). In [Section A.3.1](#), we derive the infinite-width network prior and the resulting saddle-point equations for the network's kernel. We detail the effects of partial supervision in [Section A.3.3](#) and the reduction to the standard DNN architecture in [Section A.3.4](#). The section [Section A.4](#) presents an analytical study of linear recurrent networks, deriving closed-form kernel solutions and performing a Landau analysis of the symmetry-breaking transition. Finally, we outline the numerical solution methods and provide a step-by-step summary of the derivation in [Section A.7](#).

### A.1. Setup

Recall the definition of the RNN: at each time step  $t$ , the preactivations are  $\mathbf{h}^t \in \mathbb{R}^{N \times P}$ , where  $P$  is the index over training samples. The networks have one scalar output for each training sample  $y^t \in \mathbb{R}^P$  and are updated according to

$$\begin{aligned} \mathbf{h}^t &= \mathbf{W}\phi^{t-1} + \mathbf{U}\mathbf{x}^{t-1} \quad 1 \leq t < T, \\ f^{t+1} &= \mathbf{V}\phi^t, \\ y^{t+1} &= f^{t+1} + \xi^{t+1}, \end{aligned} \tag{11}$$

where  $\mathbf{x}^t$  is the input at time  $t$  and we have defined the shorthand  $\phi^t = \phi(\mathbf{h}^t)$ . The parameters  $\mathbf{U} \in \mathbb{R}^{N \times D}$ ,  $\mathbf{W} \in \mathbb{R}^{N \times N}$ ,  $\mathbf{V} \in \mathbb{R}^{1 \times N}$  are matrices which we assume to have Gaussian priors that are i.i.d. over the matrices' entries

$$\begin{aligned} \mathbf{U} &\stackrel{\text{i.i.d.}}{\sim} \mathcal{N}_{\mathbf{U}}(\mathbf{U}) := \mathcal{N}(0, G_{\mathbf{U}}), \\ \mathbf{W} &\stackrel{\text{i.i.d.}}{\sim} \mathcal{N}_{\mathbf{W}}(\mathbf{W}) := \mathcal{N}(0, G_{\mathbf{W}}), \\ \mathbf{V} &\stackrel{\text{i.i.d.}}{\sim} \mathcal{N}_{\mathbf{V}}(\mathbf{V}) := \mathcal{N}(0, G_{\mathbf{V}}), \end{aligned} \tag{12}$$

for which our derivation will reveal the natural scalings  $G_{\mathbf{U}} =: U = u/D$ ,  $G_{\mathbf{W}} =: W = w/N$ ,  $G_{\mathbf{V}} =: V = v/N^2$  with  $\mathcal{O}(1)$  parameters  $v, w, u$ . The network output  $f^t$  is a vector  $\in \mathbb{R}^P$ . Furthermore, we assume a readout noise that is i.i.d. in time and patterns,  $\xi_p^t \stackrel{\text{i.i.d.}}{\sim} \mathcal{N}_{\mathbf{K}}(\xi_p^t) := \mathcal{N}(0, \mathbf{K})$  with  $\mathbf{K} = \kappa/N$ . We define time-advanced  $(\circ^+)^{tt'} := \circ^{t+1, t'+1}$  and time-retarded  $(\circ^-)^{tt'} := \circ^{t-1, t'-1}$  kernel matrices to ease notation. We also define the input kernel  $\mathbb{X}^{tt'} := \frac{1}{D} \sum_{i=1}^D \mathbf{x}_i^t \mathbf{x}_i^{t'}$  and the label kernel  $\mathbb{Y}^{tt'} := y^t y^{t'}$  for convenience.

### A.2. Bayesian inference and relation to training dynamics

We here derive a theory of learning that has two interpretations. The first is that of Bayesian inference. Second, as the stationary distribution of weights after training by stochastic gradient Langevin dynamics (SGLD). Both approaches will be described by the same set of equations.

**Bayesian inference** Given a set of training data  $\mathcal{D} = \{(\mathbf{x}_p^{t-1}, y_p^{t+1})\}_{1 \leq p \leq P}^{1 \leq t < T}$ , the Bayesian approach assumes a neuronal architecture, for example (11), which defines the network output as a function  $f(\Theta, \mathbf{x})$  that depends on the network's input  $\mathbf{x} \in \mathbb{R}^{T \times P \times D}$  and its parameters  $\Theta$ ; in our case,  $\Theta = \{\mathbf{W}, \mathbf{V}, \mathbf{U}\}$ . The set of all inputs is combined into the matrix  $\mathbf{x}$  and the set of outputs in a vector  $y \in \mathbb{R}^{T \times P}$ . One assumes a prior distribution  $P(\Theta)$  on the set of parameters; in our case, the distribution  $P(\Theta)$  is given by the set of distributions  $\mathcal{N}_{\mathbf{U}}(\mathbf{U}), \mathcal{N}_{\mathbf{W}}(\mathbf{W}), \mathcal{N}_{\mathbf{V}}(\mathbf{V})$  (12).

Together with the observation likelihood  $\mathcal{N}(y|f(\Theta, \mathbf{x}), \mathbf{K}\mathbb{I})$ , this defines a posterior over weights

$$P(\Theta|y, \mathbf{x}) \propto \mathcal{N}(y|f(\Theta, \mathbf{x}), \mathbf{K}\mathbb{I}) P(\Theta), \tag{13}$$

using the rules of Bayesian inference. In turn, this weight posterior induces a marginal distribution on labels  $y$

$$P(y|\mathbf{x}) = \int P(y, \Theta|\mathbf{x}) d\Theta. \tag{14}$$

We can obtain the statistics of any function  $O(\Theta)$  under the posterior over weights from the cumulant generating function (sometimes referred to as “free energy”)

$$\mathcal{W}(y, j) = \ln \int e^{j O(\Theta)} \mathcal{N}(y|f(\Theta, \mathbf{x}), K\mathbb{I}) P(\Theta) d\Theta. \quad (15)$$

For example, the mean of  $O$  follows as

$$\langle O(\Theta) \rangle_{P(\Theta|\mathbf{x}, y)} = \partial_j \mathcal{W}(y, j) \Big|_{j=0},$$

where one notes that the outer derivative of the logarithm yields the correct normalization as in (13). Higher order cumulants are obtained as higher order derivatives.

**Stochastic gradient Langevin dynamics** The second interpretation of (13) is that of a stationary distribution of a time-dependent learning rule for the weights. It is known that the stochastic differential equation

$$\begin{aligned} d\Theta(s) &= -\nabla_\Theta H(\Theta) ds + dB(s), \\ \langle dB(s)dB(s') \rangle &= \delta(s-s') \frac{2}{\beta} ds, \end{aligned} \quad (16)$$

where  $dB(t)$  is a Wiener increment, has the stationary distribution (e.g., [Gardiner \(1985\)](#); [Risken \(1996\)](#))

$$P(\Theta) \propto \exp(-\beta H(\Theta)). \quad (17)$$

For Gaussian prior measures on the weights with variance  $g$  one has  $P(\Theta) \propto \exp(-\|\Theta\|^2/2G)$ , so that (14) can be written as

$$P(y|\mathbf{x}) \propto \int \exp\left(-\frac{1}{2K}\|y - f(\Theta, \mathbf{x})\|^2 - \frac{1}{2G}\|\Theta\|^2\right) d\Theta,$$

so that we identify  $H$  in (17) as

$$H(\Theta) = \frac{PT}{K\beta} \mathcal{L}(\Theta) + \frac{1}{2G\beta} \|\Theta\|^2,$$

where the first term is expressed in terms of the the mean squared error between the given data and network output

$$\mathcal{L}(\Theta) = \frac{1}{2PT} \|y - f(\Theta, \mathbf{x})\|^2,$$

where the appearing vectors in the norm are  $\mathbb{R}^{T-P}$

Discretizing (16) in time and omitting a Metropolis-Hastings correction (MALA) [Besag \(1994\)](#), this scheme becomes identical to plain stochastic gradient descent (SGD), with the difference that the source of the noise here is i.i.d. Gaussian, whereas it is more structured mini-batch noise in typical deployments of SGD.

### A.3. Bayesian adaptive kernel theory for RNN and DNN

In this section we derive a unified mean-field formulation in kernel-space that treats deep feedforward (DNN) and recurrent (RNN) networks on the same footing. This is achieved by unrolling the RNN in time. The strategy is to treat learning as Bayesian inference and to write the network as a conditional density  $P(f|\mathbf{x})$  that is an integral over collective fields encoding pre-activation covariances, integrate out all microscopic Gaussian parameters, and then take the large-width limit  $N \rightarrow \infty$  via a saddle-point analysis. In this formulation the only structural difference between DNNs and RNNs is encoded by a simple masking operator on the time indices (equivalent to layers in the DNN case), while the scaling of the parameters and auxiliary fields with networks width  $N$  remains identical across architectures.

## A.3.1. DERIVATION OF NETWORK PRIOR

We here derive the concrete form of the network prior (14) for the architecture (11). The computation follows closely previous works Segadlo et al. (2022); Fischer et al. (2024); Lauditi et al. (2025). We also give a compact overview of the derivation in Section A.7 that emphasizes the choice of scaling.

Since the cumulants of an observable (15) over the posterior over weights can be obtained equivalently from the network prior (14) by taking the logarithm and considering suitable derivatives, it is sufficient to derive the form of the prior. To this end, it is convenient to decompose the network prior into a chain of conditional probabilities

$$P(y|\mathbf{x}) = \int \mathcal{N}(y|f', \mathbf{K} \mathbb{I}) P(f'|\mathbf{x}) df', \quad (18)$$

with

$$P(f'|\mathbf{x}) = \langle \delta(f' - f(\mathbf{U}, \mathbf{V}, \mathbf{W}, \mathbf{x})) \rangle_{\mathbf{U} \sim \mathcal{N}_{\mathbf{U}}, \mathbf{V} \sim \mathcal{N}_{\mathbf{V}}, \mathbf{W} \sim \mathcal{N}_{\mathbf{W}}}.$$

The latter can further be decomposed as

$$P(f'|\mathbf{x}) = \int P(f'|\mathbf{h}) P(\mathbf{h}|\mathbf{x}) d\mathbf{h}. \quad (19)$$

The Dirac constraint is rewritten in its Fourier representation as

$$\begin{aligned} \delta(f' - f) &\equiv \prod_{p=1}^P \prod_{t=2}^T \delta(f_p'^t - f_p^t) \\ &= \prod_{p=1}^P \prod_{t=2}^T \frac{1}{2\pi i} \int_{-i\infty}^{i\infty} d\tilde{f}_p^t \exp\left\{\tilde{f}_p^t [f_p'^t - f_p^t]\right\}, \end{aligned}$$

which allows us to compute the expectation value over  $\mathbf{V}$  as

$$\begin{aligned} P(f'|\mathbf{h}) &= \int \mathcal{D}\tilde{f} \left\langle \exp\left\{\sum_{t,p} \tilde{f}_p^t [f_p'^t - \sum_i V_i \phi_{p,i}^{t-1}] \right\} \right\rangle_{\mathbf{V} \sim \mathcal{N}_{\mathbf{V}}(0, v/N^2)} \\ &= \exp\left\{\sum_{t,p} \tilde{f}_p^t f_p'^t + \frac{1}{2} \sum_{p,p';t,t'} \tilde{f}_p^t \tilde{f}_{p'}^{t'} \frac{v}{N^2} \sum_i \phi_{p,i}^{t-1} \phi_{p',i}^{t'-1}\right\}, \end{aligned}$$

where we define the integral measure  $\int \mathcal{D}\tilde{f} = \left( \prod_{p=1}^P \prod_{t=2}^T \frac{1}{2\pi i} \int_{-i\infty}^{i\infty} d\tilde{f}_p^t \right)$ . We write the latter expression for short as

$$P(f'|\mathbf{h}) = \int \mathcal{D}\tilde{f} \exp\left\{\sum_t \tilde{f}^{t\top} f'^t + \frac{1}{2} \sum_{t,t'} \tilde{f}^{t\top} \frac{v}{N^2} [\phi^{t-1} \cdot \phi^{t'-1\top}] \tilde{f}^{t'}\right\}, \quad (20)$$

where  $\mathbf{a} \cdot \mathbf{b}$  denotes an inner product over  $i = 1, \dots, N$  and  $\mathbf{a}^\top \mathbf{b}$  an inner product over  $p = 1, \dots, P$ . We showed how we can write (18) as:

$$P(y|\mathbf{x}) = \int \left[ \int \mathcal{N}(y|f', \mathbf{K} \mathbb{I}) P(f'|\mathbf{h}) df' \right] P(\mathbf{h}|\mathbf{x}) d\mathbf{h} \quad (21)$$

Performing the integral over  $f'$ , yields

$$\begin{aligned} P(y|\mathbf{h}) &= \int \mathcal{N}(y|f', \mathbf{K} \mathbb{I}) P(f'|\mathbf{h}) df' \\ &= \int \mathcal{D}\tilde{f} \exp\left\{\sum_t \tilde{f}^{t\top} y^t + \frac{1}{2} \sum_t \frac{\kappa}{N} \tilde{f}^{t\top} \tilde{f}^t + \frac{1}{2} \sum_{t,t'} \tilde{f}^{t\top} \frac{v}{N^2} [\phi^{t-1} \cdot \phi^{t'-1\top}] \tilde{f}^{t'}\right\}, \end{aligned} \quad (22)$$

where we used the parameter  $K = \kappa/N$ . We again use the Fourier representation of the delta function to enforce the evolution of the network dynamics (11) for each sample  $p$  and each time  $t$  as

$$\begin{aligned} P(\mathbf{h}|\mathbf{x}) &= \prod_t \langle \delta(\mathbf{h}^t - \mathbf{W}^{(t-1)} \phi^{t-1} - \mathbf{U} \mathbf{x}^{t-1}) \rangle_{\mathbf{U} \sim \mathcal{N}_U, \{\mathbf{W}^{(t)}\} \sim \mathcal{N}_W} \\ &= \int \mathcal{D}\tilde{\mathbf{h}} \exp \left\{ \sum_t \tilde{\mathbf{h}}^{t\top} \cdot \mathbf{h}^t + \frac{1}{2} \sum_{t,t'} \tilde{\mathbf{h}}^t \cdot \left[ \bar{\delta}^{t-1,t'-1} \frac{w}{N} \phi^{t-1} \cdot \phi^{t'-1} + \frac{u}{D} \mathbf{x}^{t-1} \cdot \mathbf{x}^{t'-1\top} \right] \cdot \tilde{\mathbf{h}}^{t'} \right\}. \end{aligned} \quad (23)$$

Where we used the identity  $\mathbb{E}_{w \sim \mathcal{N}(0, \Sigma)} [e^{a^\top w}] = \exp\left(\frac{1}{2} a^\top \Sigma a\right)$  and introduced the symbol

$$\bar{\delta}^{tt'} = \begin{cases} \delta^{tt'} & \text{DNN} \\ 1 & \text{RNN} \end{cases}.$$

The difference arises, because for the RNN there is only a single weight matrix  $\mathbf{W}$  valid for all timesteps  $t$ , thus its entries are perfectly correlated across time, while in the DNN, the matrices  $\mathbf{W}^{(t)}$  are drawn from prior distributions which are independent across different layers  $t$ .

One notes that due to the appearance of the inner products of the fields  $\tilde{\mathbf{h}}$ , the exponent factorizes across neuron indices  $i$ , which allows us to reduce the  $N$  integrals over  $\mathbf{h}$  and  $\tilde{\mathbf{h}}$  to a single integral each. We introduce auxiliary fields for terms that contain an inner product over the neuron index, which we anticipate will concentrate in the large- $N$  limit, thus defining

$$\begin{aligned} \Phi^{tt'} &:= \frac{1}{N} \phi^t \cdot \phi^{t'\top} \in \mathbb{R}^{P \times P}, \\ \mathbb{X}^{tt'} &:= \frac{1}{D} \mathbf{x}^t \cdot \mathbf{x}^{t'\top} \in \mathbb{R}^{P \times P}. \end{aligned} \quad (24)$$

Likewise, the kernels  $\mathbb{X}_{pp'}^{tt'} := \frac{1}{D} \sum_i^D x_{p,i} x_{p',i}^{t'} \mathbb{1}$  and  $\mathbb{Y}_{pp'}^{tt'} := y_p y_{p'}^{t'} \mathbb{1}$  denote input and label kernels, and  $\mathbb{H}_{pp'}^{tt'} := \frac{1}{N} \sum_i^N h_{p,i}^t h_{p',i}^{t'} \mathbb{1}$  is the kernel for the preactivations, defined in analogy to the kernel  $\Phi$  for the postactivations. Enforcing the former definition by introducing a second auxiliary field  $\tilde{\tilde{C}} \in i\mathbb{R}^{PT \times PT}$  one inserts a Dirac constraint in the form

$$\delta(-\Phi^{tt'} + \frac{1}{N} \phi^t \cdot \phi^{t'\top}) = \int \mathcal{D}\tilde{\tilde{C}} \exp \left\{ - \sum_{t,t';p,p'} \tilde{\tilde{C}}_{pp'}^{tt'} \Phi_{pp'}^{tt'} + \tilde{\tilde{C}}_{pp'}^{t,t'} \frac{1}{N} \phi_p^t \cdot \phi_{p'}^{t'} \right\}.$$

where we used  $\int \mathcal{D}\tilde{\tilde{C}} = \left( \prod_{p,p'=1}^P \prod_{t,t'=1}^T \frac{1}{2\pi i} \int_{-i\infty}^{i\infty} dC_{pp'}^{tt'} \right)$ . This allows us to use equation (20) to write as

$$\begin{aligned} P(y|\Phi, \mathbf{x}) &= \int \mathcal{D}f \exp \left\{ f^\top y + \frac{1}{2} \sum_{t,t'} f^{t\top} \left( \frac{v}{N} \Phi^{t-1,t'-1} + \frac{\kappa}{N} \right) f^{t'} \right\}, \\ &= \exp \left\{ -\frac{N}{2} \sum_{tt'} y^{t\top} ((v\Phi^- + \kappa)^{-1})^{tt'} y^{t'} - \frac{1}{2} \ln |v\Phi^- + \kappa| + \frac{PT}{2} \ln N \right\}, \end{aligned}$$

where we performed the Gaussian integral over  $\tilde{f}$  in (22) and introduced the shorthand  $\Phi^-$  as the one time-step shifted version of the original matrix, i.e.  $(\circ^-)^{tt'} := \circ^{t-1,t'-1}$ . Inserting (23) and (23) in (21), and inserting the definitions of the auxiliary fields (24) we obtain .

$$\begin{aligned}
P(y|\mathbf{x}) &\propto \int \mathcal{D}\Phi \exp \left\{ -\frac{N}{2} \sum_{tt'} y^{t\top} ((v\Phi^- + \kappa)^{-1})^{tt'} y^{t'} + \mathcal{O}(1) \right\} \\
&\times \int \mathcal{D}\tilde{C} \exp \left\{ -\sum_{tt'} \tilde{C}^{tt'} \mathbf{1}_{\Phi^{tt'}} + N \mathcal{W}(\tilde{C}/N|\Phi, \mathbb{X}) \right\},
\end{aligned} \tag{25}$$

$$\mathcal{W}(\tilde{C}|\Phi, \mathbb{X}) := \ln \int \mathcal{D}\tilde{h} \exp \left\{ \sum_{t,t'} \phi^{t\top} \tilde{C}^{t,t'} \phi^{t'} + \sum_t \tilde{h}^{t\top} \tilde{h}^t + \frac{1}{2} \sum_{t,t'} \tilde{h}^{t\top} [\bar{\delta}^{tt'} \Phi^{t-1,t'-1} + u\mathbb{X}^{t-1,t'-1}] \tilde{h}^{t'} \right\},$$

where we used that the integrals over  $\mathbf{h}$  and over  $\tilde{\mathbf{h}}$  factorize over neurons  $i = 1 \dots N$  and thus yield the same integral to the  $N$ -th power – hence the factor  $N \mathcal{W}$  appearing and we dropped the term  $\frac{1}{2} \ln |v\Phi^- + \kappa|$  in the first line that scales as order unity on  $N$  as well as constant terms. A short way of writing the latter line is as

$$\mathcal{W}(\tilde{C}|\Phi, \mathbb{X}) := \ln \left\langle \exp \left\{ \sum_{t,t'} \sum_{p,p'} \tilde{C}_{pp'}^{tt'} \phi(h_p^t) \phi(h_{p'}^{t'}) \right\} \right\rangle_{h \sim \mathcal{N}(0, \bar{\delta}^{tt'} \Phi^{t-1,t'-1} + u\mathbb{X}^{t-1,t'-1})}, \tag{26}$$

which also corresponds to taking the integral over the  $\tilde{\mathbf{h}}$  fields.

We note that  $N \mathcal{W}(\tilde{C}/N|\Phi, \mathbb{X})$  has the form of a cumulant-generating function for the random variable  $\Phi$  and hence  $P(\Phi|\mathbb{X}) = \int \mathcal{D}\tilde{C} \exp \left( -\sum_{tt'} \tilde{C}^{tt'} \mathbf{1}_{\Phi^{tt'}} + N \mathcal{W}(\tilde{C}/N|\Phi, \mathbb{X}) \right)$  is the Fourier representation of the probability distribution  $P(\Phi|\mathbb{X})$ . The trailing factor  $N$  and the factor  $N^{-1}$  coming together with the source variable come in what is known as the scaling form – they indicate that first derivatives are  $\mathcal{O}(1)$ , while all higher derivatives are suppressed with at least  $N^{-1}$ , indicating that the mean dominates the distribution of  $\Phi$ .

An alternative way of seeing this is to define the rescaled, intensive field  $\tilde{C} := \tilde{C}/N$  which then leads to

$$\begin{aligned}
P(\Phi|\mathbb{X}) &\propto \int \mathcal{D}\tilde{C} \exp \left\{ -N \sum_{tt'} \tilde{C}^{tt'} \mathbf{1}_{\Phi^{tt'}} + N \mathcal{W}(\tilde{C}|\Phi, \mathbb{X}) \right\} \\
&\stackrel{N \rightarrow \infty}{\simeq} \exp \left\{ N \sup_{\tilde{C}} \left[ -\sum_{tt'} \tilde{C}^{tt'} \mathbf{1}_{\Phi^{tt'}} + \mathcal{W}(\tilde{C}|\Phi, \mathbb{X}) \right] \right\} \\
&=: \exp \left\{ -N \Gamma(\Phi|\mathbb{X}) \right\}.
\end{aligned} \tag{27}$$

The latter expression follows from a saddle point approximation of the Fourier integral over  $\tilde{C}$  and shows that a rate function  $\Gamma$  appears in the exponent. We note that the entire integrand appearing in (25) has a trailing factor  $N$ , so that we may also take the integral over  $\Phi$  in saddle point approximation, which leads to

$$\ln P(y|\mathbf{x})/N \simeq \sup_{\Phi} \left[ -\frac{1}{2} \sum_{tt'} y^{t\top} ((v\Phi^- + \kappa)^{-1})^{tt'} y^{t'} - \Gamma(\Phi|\mathbb{X}) \right] =: S(\Phi|\mathbb{Y}, \mathbb{X}). \tag{28}$$

This object is our main theoretical result, which recasts the problem of learning into a variational problem of determining the maximum of the right hand side with regard to  $\Phi$ .

### A.3.2. SADDLE-POINT EQUATIONS FOR THE RNN CASE

We now instantiate the RNN case by replacing  $\bar{\delta}^{tt'} = 1$  and redefine contractions  $a^T b := \sum_{tp} a_p^t b_p^t$  to run over patterns and time (unlike only patterns as before) to ease notation. The supremum condition (saddle point equation) for  $\tilde{C}$  can be obtained by taking in (27) then becomes

$$\begin{aligned}
\Phi_{pp'}^{tt'} &= \frac{\partial \mathcal{W}}{\partial \tilde{C}_{pp'}^{tt'}}(\tilde{C}|\mathbb{Y}, \mathbb{X}) = \frac{1}{Z} \langle \phi(h_p^t) \phi(h_{p'}^{t'}) \exp \{ \sum_{pp'} \sum_{tt'} \phi(h_p^t) \tilde{C}_{pp'}^{tt'} \phi(h_{p'}^{t'}) \} \rangle_{h \sim \mathcal{N}(0, w\Phi^- + u\mathbb{X}^-)} \\
&=: \langle \phi(h_p^t) \phi(h_{p'}^{t'}) \rangle_{P(h|y, \mathbf{x})},
\end{aligned}$$

where  $Z = \langle \exp\{\sum_{pp'} \sum_{tt'} \phi(h_p^t) \tilde{C}_{pp'}^{tt'} \phi(h_{p'}^{t'})\} \rangle_{h \sim \mathcal{N}(0, w\Phi^- + u\mathbb{X}^-)}$  is a the normalization constant. The expectation thus is taken with respect to the posterior  $P(h|y, \mathbf{x}) = P(h|\Phi, \tilde{C}, \mathbb{Y}, \mathbb{X})$ , i.e. the kernels  $\Phi, \tilde{C}, \mathbb{Y}, \mathbb{X}$  are sufficient statistics for this measure.

To close these equations, we still need an expression for  $\tilde{C}$ . For that we re-write the action  $S(\Phi|\mathbb{Y}, \mathbb{X}) = \sup_{\Phi} \left[ -\frac{1}{2} \text{tr}(\mathbb{Y}(v\Phi^- + \kappa)^{-1}) - \Gamma(\Phi|\mathbb{X}) \right]$  and the cumulant generating function (26)

$$\mathcal{W}(\tilde{C}|\mathbb{X}) := \ln \int dh \exp \left( -\frac{1}{2} h^T (w[\Phi^-] + u\mathbb{X}^-)^{-1} h + \phi^T \tilde{C} \phi \right) - \frac{1}{2} \ln |w[\Phi^-] + u\mathbb{X}^-|,$$

in term of kernel matrices. We had introduced the kernel  $\mathbb{H}_{pp'}^{tt'} := \frac{1}{N} \sum_i^N h_{p,i}^t h_{p',i}^{t'}$ , which we can now write as  $\mathbb{H} := \langle hh^T \rangle_{P(h|\mathbf{x}, y)}$ . Using  $\frac{\partial}{\partial \Phi^-} \ln |w[\Phi^-] + u\mathbb{X}^-| = w(w[\Phi^-] + u\mathbb{X}^-)^{-1}$  and demanding stationarity of  $S$  (28) with respect to  $\Phi$  we obtain:

$$0 \stackrel{!}{=} \frac{\partial S}{\partial \Phi} \Leftrightarrow \tilde{C} = \begin{pmatrix} \frac{1}{2} v(v\Phi^- + \kappa)^{-1} & \mathbb{Y} & 0 \\ + \frac{1}{2} w(w[\Phi^-] + u\mathbb{X}^-)^{-1} & \mathbb{H} & (w[\Phi^-] + u\mathbb{X}^-) \end{pmatrix} (v\Phi^- + \kappa)^{-1} (w[\Phi^-] + u\mathbb{X}^-)^{-1}, \quad (29)$$

..

This derivation yields the first main result of this work, cf. (3).

### A.3.3. EFFECT OF PARTIAL TEMPORAL SUPERVISION

In the derivation above we assumed that the observation noise variance  $\kappa$  is the same for all timesteps. We now generalize to partial temporal supervision, where only a subset of timesteps is observed. The key insight is probabilistic: since  $\kappa$  controls the observation noise variance, setting  $\kappa_t \rightarrow \infty$  at unobserved timesteps  $t$  makes the corresponding labels infinitely uncertain, hence uninformative. Therefore, the label-dependent term in (29) should vanish at these points.

To verify this formally, let  $\bar{\mathcal{T}}$  denote the set of unobserved timesteps and define the projector  $\mathbf{U}\mathbf{U}^T = \sum_{t \in \bar{\mathcal{T}}} \mathbf{e}_t \mathbf{e}_t^T$  onto this subspace, where  $\{\mathbf{e}_t\}_{t=1 \dots T}$  is the standard basis. The slack matrix becomes  $\kappa = \kappa(\mathbf{I}_T - \mathbf{U}\mathbf{U}^T) + \kappa_\infty \mathbf{U}\mathbf{U}^T$ . For any matrix  $\mathbf{A}$  like the ones appearing in (29), the Woodbury identity gives

$$\begin{aligned} (\mathbf{A} + \kappa_\infty \mathbf{U}\mathbf{U}^T)^{-1} &= \mathbf{A}^{-1} - \mathbf{A}^{-1} \mathbf{U} (\kappa_\infty^{-1} + \mathbf{U}^T \mathbf{A}^{-1} \mathbf{U})^{-1} \mathbf{U}^T \mathbf{A}^{-1} \\ &\xrightarrow{\kappa_\infty \rightarrow \infty} \mathbf{A}^{-1} - \mathbf{A}^{-1} \mathbf{U} (\mathbf{U}^T \mathbf{A}^{-1} \mathbf{U})^{-1} \mathbf{U}^T \mathbf{A}^{-1}. \end{aligned}$$

This expression has vanishing support on  $\text{span}\{\mathbf{e}_t\}_{t \in \bar{\mathcal{T}}}$ , as can be verified by multiplying with  $\mathbf{U}$  from the left and  $\mathbf{U}^T$  from the right. Thus the immediate 'force' in the first line of (29) due to labels vanishes at unobserved timesteps, and only the NNGP prior (second line) remains. Note that due to indirect feedback through observed points, the posterior  $\langle hh^T \rangle$  will still deviate from the NNGP prior; see Fischer et al. (2024).

### A.3.4. REDUCTION TO DNN CASE

In their standard formulation, DNNs differ from the general architecture developed in Section A.3.1 in three aspects:

1. There is only input in the first layer,  $\mathbf{x}^t = \delta^{t0} \mathbf{x}^0$ .
2. There is only output supervision on the last layer. This does not amount to just setting  $y^{t < T} = 0$ , instead, we loosen the slack in all but the last layer. This can also be interpreted as believing that hypothetical evidence  $y^{t < T}$  is non-salient (i.e., measurements that have been corrupted by uninformative noise  $\xi^{t < T} \sim \mathcal{N}(0, \kappa_\infty \mathbf{I}^{t < T})$ ,  $\kappa_\infty \gg \kappa$ ).
3. The weights under the prior are pairwise independent random variables across layers,  $P(\mathbf{W}^{(t)}, \mathbf{W}^{(t+1)}) = \mathcal{N}_{\mathbf{W}}(\mathbf{W}^{(t)}) \mathcal{N}_{\mathbf{W}}(\mathbf{W}^{(t+1)})$ . After marginalization, this amounts to masking all off-diagonal elements to be zero in the relevant expressions, denoted as  $[\Phi] \rightarrow \text{diag}(\Phi)$  (the vectorized version of replacing  $\delta^{tt'} \rightarrow \delta^{tt'}$ ), i.e. only sampling the measure in the covariance that is the diagonal of  $\Phi$ .

This leads to the following effect on the saddle-point equations,. The kernel order parameter reads

$$\Phi^{tt'} = \frac{\partial \mathcal{W}}{\partial \tilde{C}^{tt'}}(\Phi; \tilde{C}) = \langle \phi(h^t) \phi(h^{t'}) \rangle_{P(h|\Phi, \tilde{C}, \mathbb{Y}, \mathbb{X})} . \quad (30)$$

The supremum condition for  $\tilde{C}$  in (27) becomes

$$\begin{aligned} 0 \stackrel{!}{=} \frac{\partial S}{\partial \Phi} \Leftrightarrow \tilde{C} = & \frac{1}{2} v(v\Phi^- + \kappa)^{-1} \begin{pmatrix} \mathbb{Y} & - & 0 \end{pmatrix} (v\Phi^- + \kappa)^{-1} \\ & + \frac{1}{2} w(w\text{diag}(\Phi^-) + u\mathbb{X}^-)^{-1} \begin{pmatrix} \mathbb{H} & - & (w\text{diag}(\Phi^-) + u\mathbb{X}^-) \end{pmatrix} (w\text{diag}(\Phi^-) + u\mathbb{X}^-)^{-1}. \end{aligned} \quad (31)$$

The first line can be interpreted as a tilt  $\tilde{C}_y$  due to the ( $\kappa$ -regularized) constraint to match the labels  $y$ , and the second line as a tilt  $\tilde{C}_h$  due to the definition of the network's forward pass.

Due to the diagonal-only coupling, this set of equations can be reduced. To this end, we make the diagonal Ansatz  $\Phi = \text{diag}(\Phi)$ ,  $\tilde{C} = \text{diag}(\tilde{C})$ ,  $\mathbb{H} = \text{diag}(\mathbb{H})$ . Then, the conjugate saddle point equation (30) becomes

$$\begin{aligned} \tilde{C}^{TT} &= \frac{1}{2} v(v\Phi^{T-T} + \kappa)^{-1} \begin{pmatrix} \mathbb{Y}^{TT} & - & 0 \end{pmatrix} (v\Phi^{T-T} + \kappa)^{-1}, \\ \tilde{C}^{tt} &= \frac{1}{2} w(w\Phi^{t-1,t-1})^{-1} \begin{pmatrix} \langle h^t h^t \rangle & - & w\Phi^{t-1,t-1} \end{pmatrix} (w\Phi^{t-1,t-1})^{-1}, \quad 2 \leq t < T-1 \\ \tilde{C}^{11} &= \frac{1}{2} w(u\mathbb{X}^{0,0})^{-1} \begin{pmatrix} \langle h^1 h^1 \rangle & - & u\mathbb{X}^{0,0} \end{pmatrix} (u\mathbb{X}^{0,0})^{-1}, \end{aligned} \quad (32)$$

where we used  $\kappa^{\leq T} = \kappa_\infty \rightarrow \infty$ . (32) reproduces the saddle-point equations previously derived for DNNs Fischer et al. (2024); Lauditi et al. (2025).

#### A.4. Special case of linear recurrent networks

We here consider the special case of a linear activation function  $\phi(h) = h$ , in which the effective probability and saddle point equations simplify considerably.

##### A.4.1. KERNEL MEAN-FIELD THEORY FOR THE LINEAR CASE

We derived the rate function (27) and the cumulant-generating function (26), which in the linear case specialize to

$$\begin{aligned} P(\mathbb{H}|\mathbb{X}) &\propto \exp \{-N\Gamma(\mathbb{H}|\mathbb{X})\}, \quad \Gamma(\mathbb{H}|\mathbb{X}) = \sup_{\tilde{C}} \left( \text{tr } \tilde{C}^\top \mathbb{H} - \mathcal{W}(\tilde{C}|\mathbb{X}) \right), \\ \mathcal{W}(\tilde{C}|\mathbb{X}) &= \ln \int dh \exp \left\{ -\frac{1}{2} h^\top (w\mathbb{H}^- + u\mathbb{X}^-)^{-1} h + h^\top \tilde{C} h - \frac{1}{2} N \ln |w\mathbb{H}^- + u\mathbb{X}^-| \right\}. \end{aligned}$$

Using the supremum condition for  $\tilde{C}$  in (27)

$$0 \stackrel{!}{=} \frac{d}{d\tilde{C}} \left( \tilde{C}^\top \mathbb{H} - \mathcal{W}(\tilde{C}|\mathbb{X}) \right) \Leftrightarrow \tilde{C}(\mathbb{H}) = \frac{1}{2} (w\mathbb{H}^- + u\mathbb{X}^-)^{-1} - \frac{1}{2} \mathbb{H}^{-1},$$

we get by plugging in

$$\begin{aligned} \Gamma(\mathbb{H}|\mathbb{X}) &= \text{tr } \tilde{C}(\mathbb{H})^\top \mathbb{H} - \mathcal{W}(\tilde{C}(\mathbb{H})|\mathbb{X}) \\ &= \frac{1}{2} \text{tr} [\mathbb{H} \left( (w\mathbb{H}^- + u\mathbb{X}^-)^{-1} - \mathbb{H}^{-1} \right)] - \ln \int dh \exp \left\{ -\frac{1}{2} h^\top (w\mathbb{H}^- + u\mathbb{X}^-)^{-1} h + h^\top \tilde{C} h \right. \\ &= \frac{1}{2} \text{tr} [\mathbb{H} (w\mathbb{H}^- + u\mathbb{X}^-)^{-1} - \mathbb{I}] - \ln \int dh \exp \left\{ -\frac{1}{2} h^\top (w\mathbb{H}^- + u\mathbb{X}^-)^{-1} h + \frac{1}{2} h^\top \left( (w\mathbb{H}^- + u\mathbb{X}^-)^{-1} - \mathbb{H}^{-1} \right) h \right. \\ &= \frac{1}{2} \text{tr} [\mathbb{H} (w\mathbb{H}^- + u\mathbb{X}^-)^{-1} - \mathbb{I}] - \ln \int dh \exp \left\{ -\frac{1}{2} h^\top \mathbb{H}^{-1} h \right. \\ &\stackrel{+\text{const.}}{=} \frac{1}{2} \text{tr} [\mathbb{H} (w\mathbb{H}^- + u\mathbb{X}^-)^{-1}] \end{aligned} \quad (33)$$

where we note that  $\frac{1}{2}\text{tr}[\mathbb{H}(w\mathbb{H}^- + u\mathbb{X}^-)^{-1}] - \frac{1}{2}\ln\frac{|\mathbb{H}|}{|w\mathbb{H}^- + u\mathbb{X}^-|} = D_{\text{KL}}\left(\mathcal{N}_h(0, \mathbb{H}) \parallel \mathcal{N}_h(0, w[\mathbb{H}^-] + u\mathbb{X}^-)\right)$  is the Kullback-Leibler divergence between two Gaussians in  $h \in \mathbb{R}^T$ . Note that this result can also be obtained directly from noticing that the supremum condition on  $\tilde{C}$  is made precisely such that  $\mathbb{H} = \langle hh^\top \rangle$  (by definition of the Legendre transform). Hence the integral over  $h$  is a Gaussian with covariance  $\mathbb{H}$ .

#### A.4.2. CLOSED-FORM SOLUTION

Similarly to previous work, we can devise a closed-form solution for the kernels by eliminating  $\tilde{C}$ . The basic reason this is possible is that per (31)

$$\tilde{C} = \frac{1}{2}w(w[\mathbb{H}] + u\mathbb{X})^{-1} \left( [hh^\top]_{\Phi, \tilde{C}^+}^+ - (w[\mathbb{H}] + u\mathbb{X}) \right) (w[\mathbb{H}] + u\mathbb{X})^{-1} + \frac{1}{2}v(v\mathbb{H} + \kappa)^{-1}\mathbb{Y}^+(v\mathbb{H} + \kappa)^{-1},$$

and we in turn know that at the saddle it holds that  $\Phi^+ = [hh^\top]_{\Phi, \tilde{C}^+}^+$  giving

$$\tilde{C} = \frac{1}{2}w(w[\mathbb{H}] + u\mathbb{X})^{-1} \left( \mathbb{H}^+ - (w[\mathbb{H}] + u\mathbb{X}) \right) (w[\mathbb{H}] + u\mathbb{X})^{-1} + \frac{1}{2}v(v\mathbb{H} + \kappa)^{-1}\mathbb{Y}^+(v\mathbb{H} + \kappa)^{-1}.$$

Finally, for the linear case we can read-off  $\Phi$  directly as the coefficient of  $h$  in the action, giving  $(w[\mathbb{H}^-] + u\mathbb{X}^-)^{-1} - 2\tilde{C} = \mathbb{H}^{-1}$ . This gives a **closed-form relation** for  $\mathbb{H}$

$$\begin{aligned} (w[\mathbb{H}^-] + u\mathbb{X}^-)^{-1} - \mathbb{H}^{-1} &= w(w[\mathbb{H}] + u\mathbb{X})^{-1} \left( \mathbb{H}^+ - (w[\mathbb{H}] + u\mathbb{X}) \right) (w[\mathbb{H}] + u\mathbb{X})^{-1} \\ &\quad + v(v\mathbb{H} + \kappa)^{-1}\mathbb{Y}^+(v\mathbb{H} + \kappa)^{-1} \end{aligned} \quad (34)$$

where the last layer's term  $2\tilde{C}_h^{TT} = \mathbb{H}^{TT} - w\Phi^{T,T^-} = 0$  because the last layer is free to vary marginally.

This result of course corresponds to the stationary point of (28) in the special case of using (33)

$$S(\mathbb{H}|\mathbb{Y}, \mathbb{X}) = -\frac{1}{2}\text{tr}[\mathbb{Y}(v\mathbb{H}^- + \kappa)^{-1}] - \frac{1}{2}\text{tr}[\mathbb{H}(w\mathbb{H}^- + u\mathbb{X}^-)^{-1}] + \frac{1}{2}\ln\frac{|\mathbb{H}|}{|w\mathbb{H}^- + u\mathbb{X}^-|}.$$

#### A.4.3. PERTURBATIVE SOLUTION

We here derive the perturbative to solution to (34) that we used in Section 3.3 in the main text. For the NNGP solution (i.e., absence of learning signal  $\mathbb{Y}$ ), we have  $\mathbb{H}_0 = w[\mathbb{H}_0^-] + u\mathbb{X}^-$ . We then make a perturbation expansion  $\mathbb{H} = \mathbb{H}_0 + \Delta$ ,  $\Delta = \Delta_1 + \Delta_2 + \dots$ , where every order groups powers of  $\mathbb{Y}$ . We perform this expansion up to second order, which is the minimal order at which the architecture-dependent effects that we are interested in appear. Thus, we insert the perturbative ansatz into (34) to get the expression

$$(w(\mathbb{H}_0 + \Delta)^- + u\mathbb{X}^-)^{-1} - (\mathbb{H}_0 + \Delta)^{-1} = w(w[\mathbb{H}_0 + \Delta] + u\mathbb{X})^{-1}(\Delta^+ - w[\Delta]) (w[\mathbb{H}_0 + \Delta] + u\mathbb{X})^{-1} + v(v(\mathbb{H}_0 + \Delta) + \kappa)^{-1}\mathbb{Y}^+(v(\mathbb{H}_0 + \Delta) + \kappa)^{-1}$$

and group terms in zeroth, first, and second order in  $\mathbb{Y}$  to compare coefficients.

**Zeroth order** The terms of zeroth order

$$(w\mathbb{H}_0^- + u\mathbb{X}^-)^{-1} - \mathbb{H}_0^{-1} = 0$$

are fulfilled by having chosen the NNGP solution as the expansion point, for which  $[\mathbb{H}_0] = \mathbb{H}_0$ .

**First order** To ease notation, we introduce the NNGP ‘‘propagators’’  $\mathbb{G}_h := (w\mathbb{H}_0^- + u\mathbb{X}^-)^{-1} \equiv (\mathbb{H}_0)^{-1}$ ,  $\mathbb{G}_h^+ := (w\mathbb{H}_0 + u\mathbb{X})^{-1}$ ,  $\mathbb{G}_y := (v\mathbb{H}_0 + \kappa)^{-1}$ . Expanding the LHS resolvents and the RHS linear terms yields the defining equation for  $\Delta_1$ :

$$-(\mathbb{G}_h w[\Delta_1^-] \mathbb{G}_h - \mathbb{G}_h \Delta_1 \mathbb{G}_h) = w\mathbb{G}_h^+ (\Delta_1^+ - w[\Delta_1]) \mathbb{G}_h^+ + v\mathbb{G}_y \mathbb{Y}^+ \mathbb{G}_y,$$

where we used  $[\mathbb{H}_0] = \mathbb{H}_0$  because the NNGP solution is diagonal Segadlo et al. (2022). This moreover reveals that the first order change is proportional to  $\mathbb{Y}$ .

**Second order** Grouping second-order terms  $(\Delta_1)^2, \Delta_2$ , we get

$$\begin{aligned}
& -(\mathbb{G}_h w \llbracket \Delta_2^- \rrbracket \mathbb{G}_h - \mathbb{G}_h \Delta_2 \mathbb{G}_h) = & w \mathbb{G}_h^+ (\Delta_2^+ - w \llbracket \Delta_2 \rrbracket) \mathbb{G}_h^+ \\
& + \mathbb{G}_h w \llbracket \Delta_1^- \rrbracket \mathbb{G}_h w \llbracket \Delta_1^- \rrbracket \mathbb{G}_h - \mathbb{G}_h \Delta_1 \mathbb{G}_h \Delta_1 \mathbb{G}_h & - w (\mathbb{G}_h^+ w \llbracket \Delta_1 \rrbracket \mathbb{G}_h^+ (\Delta_1^+ - w \llbracket \Delta_1 \rrbracket) \mathbb{G}_h^+ + (\sim)^\top) \\
& & - v (\mathbb{G}_y v \Delta_1 \mathbb{G}_y \mathbb{Y}^+ \mathbb{G}_y + (\sim)^\top),
\end{aligned}$$

where  $(\sim)^\top$  denotes the transpose of the preceding term. Notably, in the second line, masked  $\llbracket \Delta_1 \rrbracket$  and unmasked  $\Delta_1$  terms appear in a product, giving rise to the contractions in the main text that allow for signal propagation.

#### A.4.4. SOLUTION DEGENERACY IN LINEAR RNNs

Within the temporally-coherent phase of endpoint-supervised tasks, there can technically also be other solutions, for example where the hidden layer activity flips sign from one timestep to the next,  $\mathbf{h}^{t+1} = -\mathbf{h}^t$ . Such solutions are unstable, since they would be suppressed by an infinitesimal residual pathway (memory term) in (1),  $\mathbf{h}^{t+1} = \dots + (1 - \alpha)\mathbf{h}^t$ . To exclude this solution, we start learning from a small  $\alpha$ , which we subsequently anneal to zero.

### A.5. Analytics for temporally coherent phase in 4-layer linear RNNs in terms of label strength

**Setup** We consider the case  $T = 4$  with  $\kappa = 0$ . Let  $\mathbb{H}_{0:4} \in \mathbb{R}^{4 \times 4}$  be the kernel and  $\mathbb{X}_{0:4}^- \in \mathbb{R}^{4 \times 4}$  encode input correlations. Here, we are adopted Python-like slicing conventions that include the first and exclude the last index of a slice, i.e.  $1:4 := (1, 2, 3)$ , and will put temporal indices into subscripts to avoid confusion with exponents. We work in the endpoint-supervised setting where in addition input is only supplied to the first layer, so

$$\mathbb{X}^- = \text{diag}(1, 0, 0, 0) = \mathbf{e}_0 \mathbf{e}_0^\top. \quad (35)$$

Moreover, we consider a single training sample, i.e.  $P = 1$ .

The log-probability (effective action) from (28) using (33) for the end-point supervised task with label  $y_4$  can be written as

$$\ell(\mathbb{H}) := \ln P(\mathbb{H}|y, \mathbf{x})/N = -\frac{1}{2} [y_4^2 (v \mathbb{H}^{T-T} + \kappa)^{-1}] - \frac{1}{2} \text{tr}[\mathbb{H}(\Sigma_h(\mathbb{H}))^{-1}] + \frac{1}{2} \ln \frac{|\mathbb{H}|}{|\Sigma_h(\mathbb{H})|}, \quad (36)$$

where we introduced the shorthand  $\Sigma_h(\mathbb{H}) = w \mathbb{H}^- + u \mathbb{X}^-$  and used that, due to the supervision of the end point only, the probability of the label  $y_4$  is with regard to the marginal distribution in the last layer alone (this is consistent with the consideration in Section A.3.3, sending the regularization noise  $\kappa \rightarrow \infty$  for all unobserved timesteps). We will use the dimensionless control parameter

$$\lambda := \frac{y_4^2}{u w^2 v}. \quad (37)$$

**Parameterization of the relevant  $3 \times 3$  block** In the  $T = 4$  case, the nontrivial dependence of  $\ell$  on off-diagonal elements is confined to the lower-right  $3 \times 3$  block of  $\mathbb{H}$ , corresponding to times 1, 2, 3. We denote this block by  $\mathbb{H}_{1:4} \in \mathbb{R}^{3 \times 3}$  and explicitly parametrize it as

$$\mathbb{H}_{1:4} = \begin{bmatrix} a & b_2 & b_3 \\ b_2 & c & d \\ b_3 & d & e \end{bmatrix}, \quad \mathbb{H}_{1:3} := \begin{bmatrix} a & b_2 \\ b_2 & c \end{bmatrix}, \quad \mathbb{H}_{2:4} = \begin{bmatrix} c & d \\ d & e \end{bmatrix}.$$

The observed output at the final time is  $y_4$ , so that  $v \mathbb{H}_{3,3} = v e$ .

For the reduced  $3 \times 3$  problem, the latent covariance over the last three times decomposes into a driven  $1 \times 1$  block and an interior  $2 \times 2$  block. The only architecture-dependent difference (RNN vs. DNN) is whether the interior block inherits the off-diagonal  $b_2$ :

$$\Sigma_h(\mathbb{H}) = \begin{cases} u \mathbf{e}_0 \mathbf{e}_0^\top \oplus w \mathbb{H}_{1:3} = \begin{bmatrix} u & 0 & 0 \\ 0 & w a & w b_2 \\ 0 & w b_2 & w c \end{bmatrix} & \text{RNN (unmasked)} \\ u \mathbf{e}_0 \mathbf{e}_0^\top \oplus w \text{diag}(\mathbb{H}_{1:3}) = \begin{bmatrix} u & 0 & 0 \\ 0 & w a & 0 \\ 0 & 0 & w c \end{bmatrix} & \text{DNN (masked)} \end{cases}, \quad (38)$$

where we used the input kernel (35) and employed  $\mathbf{e}_0 = (1, 0, 0)^\top$  in the reduced 3-dimensional indexing.

**Diagonal first-order conditions at  $b_2 = b_3 = d = 0$**  On the purely diagonal ansatz  $(b_2, b_3, d) = (0, 0, 0)$ , the RNN and DNN coincide. The saddle point conditions  $\frac{\partial}{\partial \{a, c\}} \ell(\mathbb{H}(a, c, e)) \stackrel{!}{=} 0$  then imply

$$a^2 = \frac{u}{w} c, \quad e = \frac{c^2}{a}. \quad (39)$$

We denote these stationarity conditions as “first-order-conditions” (FOC) in the following. The  $e$ -FOC  $\frac{\partial}{\partial e} \ell(\mathbb{H}(a, c, e)) \stackrel{!}{=} 0$  reduces to a scalar relation between  $e, c$  and the label:

$$\frac{1}{e} - \frac{1}{w c} + \frac{y_4^2}{v e^2} = 0. \quad (40)$$

These diagonal relations will later be used to locate the critical point in terms of  $\lambda$ .

**Architecture-dependent gradient and linear response of interior off-diagonals** The first-order condition with respect to the interior off-diagonal  $b_2$  differs between the RNN and DNN because  $\Sigma_h(\mathbb{H})$  in (38) depends on  $b_2$  only for the RNN. Writing the derivative by the matrix  $\Sigma_h$  as

$$\frac{\partial \ell}{\partial \Sigma_h} = \frac{1}{2} \Sigma_h^{-1} (\mathbb{H} - \Sigma_h) \Sigma_h^{-1},$$

the chain-rule gives

$$\partial_{b_2} \ell = (\mathbb{H}^{-1})_{12} + \begin{cases} {}^w(\Sigma_h^{-1}(\mathbb{H} - \Sigma_h)\Sigma_h^{-1})_{23}, & \text{RNN}, \\ 0, & \text{DNN}. \end{cases}$$

Here we used two properties: first, that the first term of  $\ell(\mathbb{H})$  does not depend on  $b_2$ , because it is  $-\frac{1}{2} [y_4^2 (v \mathbb{H}^{T-T} + \kappa)^{-1}]$ , which only depends on  $e$ . Second, the trace can be explicitly calculated as  $\text{tr}[\mathbb{H}(\Sigma_h(\mathbb{H}))^{-1}] = \text{sum}(\begin{bmatrix} a & b_2 & b_3 \\ b_2 & c & d \\ b_3 & d & e \end{bmatrix} \odot \begin{bmatrix} 1/u & 0 & 0 \\ 0 & w c / |\mathbb{H}_{1:3}| & -w b_2 / |\mathbb{H}_{1:3}| \\ 0 & -w b_2 / |\mathbb{H}_{1:3}| & w a / |\mathbb{H}_{1:3}| \end{bmatrix})$ , where we leveraged a block-inversion formula for  $(\Sigma_h(\mathbb{H}))^{-1}$  and used  $\text{tr}[AB] = \sum_{ij} A_{ij} B_{ij} =: \text{sum}(A \odot B)$ ; thus the  $b_2$  dependence through  $\mathbb{H}$  in the first term vanishes.

Thus only in the RNN is there an additional feedback term driven by the mismatch  $\mathbb{H} - \Sigma_h$ .

To analyze the onset of an interior off-diagonal  $d$  near the diagonal point  $(b_2, b_3, d) = (0, 0, 0)$ , we treat the off-diagonal entries  $(d, b_2, b_3)$  as small and use Schur-complement identities for  $\mathbb{H}^{-1}$ . A direct calculation gives

$$(\mathbb{H}^{-1})_{13} = \frac{-b_2 d + b_3 c}{|\mathbb{H}|}.$$

The FOC  $\partial_{b_3} \ell = (\mathbb{H}^{-1})_{13} = 0$  therefore enforces

$$b_3 = \frac{d}{c} b_2,$$

so  $b_3$  is slaved to  $b_2$  and  $d$  in a neighborhood of the diagonal manifold.

We now parameterize the linear response of  $b_2$  to  $d$  by a coefficient  $\alpha$ ,

$$b_2 = \alpha d + O(d^3),$$

and determine  $\alpha$  by enforcing the  $b_2$ -FOC. Substituting  $b_3 = (d/c) b_2$  and  $b_2 = \alpha d$  into  $\partial_{b_2} \ell = 0$  and expanding to leading order in  $d$  yields

$$\alpha = \begin{cases} \frac{ac}{c^2 + ae}, & \text{RNN}, \\ 0, & \text{DNN}. \end{cases}$$

Consequently, near the diagonal manifold,

$$b_2 = \alpha d + O(d^3), \quad b_3 = \frac{\alpha}{c} d^2 + O(d^4) \quad (\text{RNN}), \quad b_2 = b_3 = 0 \quad \text{to these orders (DNN)}.$$

**Quadratic curvature along the interior off-diagonal** We now substitute

$$b_2 = \alpha d, \quad b_3 = \frac{d}{c} b_2$$

back into  $\ell$  and expand in powers of  $d$ . The resulting Landau expansion has the form

$$\ell(d) = \ell_0 + \frac{1}{2} C^{(2)}(\alpha) d^2 - \frac{1}{4} \frac{d^4}{c^2 e^2} + \dots, \quad (41)$$

with

$$C^{(2)}(\alpha) = -\frac{1}{ce} + \frac{\alpha}{wac} \quad \Rightarrow \quad \boxed{C_{\text{RNN}}^{(2)} = -\frac{1}{ce} + \frac{1}{w(c^2 + ae)}, \quad C_{\text{DNN}}^{(2)} = -\frac{1}{ce} (< 0)}. \quad (42)$$

The term  $-\frac{1}{ce}$  is the entropic penalty from  $\ln |\mathbb{H}|$  (Hadamard inequality: at fixed diagonal, the determinant  $|\mathbb{H}|$  is maximized when off-diagonals vanish). The quartic coefficient  $-1/(4c^2 e^2)$  is architecture-independent and makes  $-\ell$  locally stabilizing.

**Critical diagonals for the RNN** A continuous transition occurs when the quadratic coefficient  $C_{\text{RNN}}^{(2)}$  changes sign. The critical point is defined by

$$C_{\text{RNN}}^{(2)} = 0 \iff w(c^2 + ae) = ce.$$

Combining this with the diagonal relations (39),

$$a^2 = \frac{u}{w} c, \quad e = \frac{c^2}{a},$$

one obtains the criticality condition for three variables

$$\boxed{a^* = 2u, \quad c^* = 4uw, \quad e^* = 8uw^2}. \quad (43)$$

At  $(a^*, c^*, e^*)$  the RNN is marginal in the direction of the interior off-diagonal  $d$ . In contrast, in the DNN one always has  $C_2^{\text{DNN}} < 0$ , so the mode remains strictly massive and no such transition occurs.

**Exact critical label strength in terms of  $\lambda$**  Plugging (43) into the  $e$ -FOC (40) gives at criticality

$$\frac{1}{e^*} - \frac{1}{wc^*} + \frac{y_4^{*2}}{v(e^*)^2} = 0.$$

Using  $c^* = 4uw$  and  $e^* = 8uw^2$ , one has  $1/(wc^*) = 2/e^*$ , so the bracket simplifies to

$$-\frac{1}{e^*} + \frac{y_4^{*2}}{v(e^*)^2} = 0 \iff y_4^{*2} = ve^* = 8uw^2.$$

Equivalently, in terms of the dimensionless control parameter (37),

$$\boxed{\lambda^* = \frac{y_4^{*2}}{uw^2 v} = 8}. \quad (44)$$

Since the label enters only through  $y_4^2$ , the sign of  $y_4$  is irrelevant for the transition. For  $\lambda < 8$ , one has  $C_{\text{RNN}}^{(2)} < 0$  and the unique maximizer is  $d^* = 0$ ; for  $\lambda > 8$ , one has  $C_{\text{RNN}}^{(2)} > 0$  and two symmetric non-zero maximizers  $\pm d^* \neq 0$  appear.

**Scaling near criticality without auxiliary variables** Eliminating the diagonal displacement in favor of  $\lambda - 8$  gives a linear expansion

$$C^{(2)}(\lambda) = K_\lambda (\lambda - 8) + o(\lambda - 8), \quad K_\lambda = \frac{1}{1280 u^2 w^3}.$$

Maximizing  $\ell(d)$  in (41) away from  $d = 0$  yields

$$d^{*2} = C^{(2)} c^2 e^2.$$

Evaluating  $c^2 e^2$  at the critical diagonals (43) gives  $c^{*2} e^{*2} = 1024 u^4 w^6$ , hence

$$d^{*2} = \frac{4}{5} u^2 w^3 (\lambda - 8) + o(\lambda - 8) \quad (\lambda \downarrow 8^+).$$

(45)

Equivalently,  $d^* = \pm \sqrt{\frac{4}{5} u^2 w^3 (\lambda - 8)} + o(\sqrt{\lambda - 8})$ , i.e. the usual mean-field exponent  $\beta = \frac{1}{2}$  for  $d$ .

For the concrete choice  $u = v = w = 1$ , one has  $\lambda = y_4^2$ ,  $\lambda^* = 8$ , and

$$d^{*2} = \frac{4}{5} (\lambda - 8) + o(\lambda - 8).$$

#### A.6. Numerical solution of kernels for saddle point equations

We here describe how to obtain the maximum a posteriori kernels that describe converged training for the linear kernels  $\mathbb{H}$  (7) and nonlinear kernels  $\Phi, \tilde{C}$  (3). For both solvers, we initialize the kernels at the NNGP solution and add a slight off-diagonal for  $\mathbb{H}$  and  $\Phi$  to break symmetry.

**Linear case** We use SciPy’s Newton-CG optimizer, a second-order method that leverages Hessian-vector products for efficient curvature approximation without forming the full Hessian. Gradients and Hessian-vector products are computed via automatic differentiation in JAX.

**Nonlinear case** The GD solver iteratively refines the kernels  $(\Phi, \tilde{C})$  by computing gradients of the free energy  $S := \ln P(\Phi, \tilde{C})$  through two passes: a “forward pass” that evaluates the feature moments at the *equilibrium* kernels  $(\mathbb{H}_{\text{eq}}^+ = \langle h^+ h^{+\top} \rangle_{(\Phi, \tilde{C})}, \Phi_{\text{eq}}^+ = \langle \phi(h^+) \phi(h^{+\top}) \rangle_{(\Phi, \tilde{C})})$  under a tilted Gaussian measure parameterized by the current solver state  $(\Phi, \tilde{C})$ , and a “backward pass” that computes the equilibrium dual kernels  $\tilde{C}_{\text{eq}}^-$  via matrix inversions. The gradients take the symmetric form

$$\begin{aligned} \nabla_\Phi S &= \tilde{C} - \tilde{C}_{\text{eq}}, \\ \nabla_{\tilde{C}} S &= \Phi - \Phi_{\text{eq}}. \end{aligned}$$

We perform gradient *descent* in  $\Phi$ , projecting the gradient to preserve positive definiteness, and gradient *ascent* in  $\tilde{C}$ . We perform these updates using an extragradient scheme that recomputes gradients at half steps.

#### A.7. Overview table of mean-field derivation

In this section, we give a compact overview of the derivation in Section A.3.1 to give a clearly traceable route through the derivation, with definitions given there. In particular, this will reveal why the chosen intensive scaling of the prior variances yields a well-defined set of saddle point equations, explaining why the chosen order parameters concentrate. We will adopt a “greedy” version of Einstein summation convention, where summations should be placed as tightly as possible around repeated indices. We will here not explicitly write out contractions over indices  $p = 1 \dots P$  for clarity. We will also assume  $P, T \ll N$  and drop any such subleading terms.

Below we make a step-by-step derivation of the network’s prior predictive distribution (14)

$$\begin{aligned} P(y|\mathbf{x}) &= \int d\mathbf{U} d\mathbf{W} d\mathbf{V} P(\mathbf{U}) P(\mathbf{W}) P(\mathbf{V}) \\ &\quad \times \int d\mathbf{h} d\xi P(\xi^t) \prod_t^T P(y^t | \mathbf{h}^{t-1}, \mathbf{V}, \xi^t) \prod_t^T P(\mathbf{h}^t | \mathbf{h}^{t-1}, \mathbf{x}^{t-1}, \mathbf{U}, \mathbf{W}), \end{aligned}$$

where  $\mathbf{h} \in \mathbb{R}^{T-P \times N}$ ,  $\xi \in \mathbb{R}^{TP}$ .

$$\begin{aligned}
& \stackrel{P(y|\mathbf{x})}{=} \int_{\mathbf{h}\xi} \int_{UWV} \delta \begin{pmatrix} y^t \\ \mathbf{h}^t \end{pmatrix} \begin{pmatrix} -(\mathbf{V}\phi^{t-1}) \\ -(\mathbf{W}^{(t-1)}\phi^{t-1}) \\ \mathcal{N}_U(\mathbf{U})\mathcal{N}_W(\{\mathbf{W}^{(t)}\}_t) \end{pmatrix} \begin{pmatrix} +\xi^{t-1} \\ +\mathbf{U}\mathbf{x}^{t-1} \\ \mathcal{N}_K(\xi) \end{pmatrix} \\
& \stackrel{1}{=} \int_{\mathbf{h}\xi\tilde{\mathbf{h}}\tilde{f}} \int_{UWV} \exp \left\{ \begin{array}{l} \iota\tilde{f}^t y^t \\ \iota\tilde{h}^t \mathbf{h}^t \end{array} \right\} \begin{pmatrix} -\tilde{f}^t \mathbf{V}\phi^{t-1} \\ -\tilde{h}^t \mathbf{W}^{(t-1)}\phi^{t-1} \\ \mathcal{N}_U(\mathbf{U})\mathcal{N}_W(\{\mathbf{W}^{(t)}\}_t) \end{pmatrix} \begin{pmatrix} -\iota\tilde{f}^t \xi^t \\ -\iota\tilde{h}^t \mathbf{U}\mathbf{x}^{t-1} \\ \mathcal{N}_K(\xi) \end{pmatrix} \\
& \stackrel{2}{=} \int_{\mathbf{h}\tilde{\mathbf{h}}\tilde{f}} \exp \left\{ \begin{array}{l} \iota\tilde{f}^t y^t \\ \iota\tilde{h}_i^t \mathbf{h}_i^t \end{array} \right\} \begin{pmatrix} -\frac{1}{2}\tilde{f}^t (\mathbf{V}\phi_i^{t-1}\phi_i^{t'-1})\tilde{f}^{t'} \\ -\tilde{h}_i^t (W\delta^{ts}\phi_j^{t-1}\phi_j^{t'-1})\tilde{h}_i^{t'} \\ \mathcal{N}_U(\mathbf{U})\mathcal{N}_W(\{\mathbf{W}^{(t)}\}_t) \end{pmatrix} \begin{pmatrix} -\frac{1}{2}\tilde{f}^t \mathbf{K}_\delta^{tt'}\tilde{f}^{t'} \\ -\frac{1}{2}\tilde{h}_i^t (Ux_j^{t-1}x_j^{t'-1})\tilde{h}_i^{t'} \\ \mathcal{N}_K(\xi) \end{pmatrix} \\
& \stackrel{3}{=} \int_{\Phi\tilde{C}} \exp \left\{ -\tilde{C}^{tt'}\Phi^{tt'} \right\} \int_{\mathbf{h}\tilde{\mathbf{h}}\tilde{f}} \exp \left\{ \begin{array}{l} \iota\tilde{f}^t y^t \\ \iota\tilde{h}_i^t \mathbf{h}_i^t \end{array} \right\} \begin{pmatrix} -\frac{1}{2}\tilde{f}^t (VN\Phi^{t-1,t'-1})\tilde{f}^{t'} \\ -\frac{1}{N}\phi_i^t \tilde{C}^{tt'}\phi_i^{t'} \\ -\tilde{h}_i^t (NW\delta^{tt'}\Phi^{t-1,t'-1})\tilde{h}_i^{t'} \end{pmatrix} \begin{pmatrix} -\frac{1}{2}\tilde{f}^t \mathbf{K}_\delta^{tt'}\tilde{f}^{t'} \\ -\tilde{h}_i^t (DU\mathbb{X}^{t-1,t'-1})\tilde{h}_i^{t'} \end{pmatrix} \\
& \stackrel{4}{=} \int_{\Phi\tilde{C}} \exp \left\{ -\tilde{C}^{tt'}\Phi^{tt'} \right\} \int_{\mathbf{h}\tilde{\mathbf{h}}\tilde{f}} \exp \left\{ \begin{array}{l} \iota N\tilde{f}^t y^t \\ \iota\tilde{h}_i^t \mathbf{h}_i^t \end{array} \right\} \begin{pmatrix} -\frac{1}{2}N^2\tilde{f}^t (VN\Phi^{t-1,t'-1})\tilde{f}^{t'} \\ -\frac{1}{N}\phi_i^t \tilde{C}^{tt'}\phi_i^{t'} \end{pmatrix} \begin{pmatrix} -\frac{1}{2}N^2\tilde{f}^t \mathbf{K}_\delta^{tt'}\tilde{f}^{t'} \\ -\tilde{h}_i^t (NW\delta^{tt'}\Phi^{t-1,t'-1})\tilde{h}_i^{t'} \end{pmatrix} \begin{pmatrix} -\frac{1}{2}N\tilde{h}_i^t (DU\mathbb{X}^{t-1,t'-1})\tilde{h}_i^{t'} \end{pmatrix} \\
& \stackrel{5}{=} \int_{\Phi\tilde{C}} \exp \left\{ -\tilde{C}^{tt'}\Phi^{tt'} \right\} \int_{\tilde{f}} \exp \left\{ \begin{array}{l} \iota N\tilde{f}^t y^t \\ \iota\tilde{h}_i^t \mathbf{h}_i^t \end{array} \right\} \begin{pmatrix} -\frac{1}{2}N^2\tilde{f}^t (VN\Phi^{t-1,t'-1})\tilde{f}^{t'} \\ \frac{1}{N}\phi_i^t \tilde{C}^{tt'}\phi_i^{t'} \end{pmatrix} \begin{pmatrix} -\frac{1}{2}N^2\tilde{f}^t \mathbf{K}_\delta^{tt'}\tilde{f}^{t'} \\ -\tilde{h}_{t,i}^t (NW\delta^{tt'}\Phi^{t-1,t'-1})\tilde{h}_i^{t'} \end{pmatrix} \begin{pmatrix} -\frac{1}{2}N\tilde{h}_i^t (DU\mathbb{X}^{t-1,t'-1})\tilde{h}_i^{t'} \end{pmatrix} \\
& \stackrel{6}{=} \int_{\Phi\tilde{C}} \exp \left\{ -\tilde{C}^{tt'}\Phi^{tt'} \right\} \int_{\tilde{f}} \exp \left\{ \begin{array}{l} \iota N\tilde{f}^t y^t \\ \iota\tilde{h}^t \mathbf{h}^t \end{array} \right\} \begin{pmatrix} -\frac{1}{2}N^2\tilde{f}^t (VN\Phi^{t-1,t'-1})\tilde{f}^{t'} \\ \phi^t \tilde{C}^{tt'}\phi^{t'} \end{pmatrix} \begin{pmatrix} -\frac{1}{2}N^2\tilde{f}^t \mathbf{K}_\delta^{tt'}\tilde{f}^{t'} \\ -\tilde{h}^t (NW\delta^{tt'}\Phi^{t-1,t'-1})\tilde{h}^{t'} \end{pmatrix} \begin{pmatrix} -\frac{1}{2}\tilde{h}^t (DU\mathbb{X}^{t-1,t'-1})\tilde{h}^{t'} \end{pmatrix} \\
& \stackrel{7}{=} \int_{\Phi\tilde{C}} \exp \left\{ -N\tilde{C}^{tt'}\Phi^{tt'} \right\} \int_{\tilde{f}} \exp \left\{ \begin{array}{l} \iota N\tilde{f}^t y^t \\ \iota\tilde{h}^t \mathbf{h}^t \end{array} \right\} \begin{pmatrix} -\frac{1}{2}N\tilde{f}^t (\mathbf{v}\Phi^{-1,t'-1})\tilde{f}^{t'} \\ \phi^t \tilde{C}^{tt'}\phi^{t'} \end{pmatrix} \begin{pmatrix} -\frac{1}{2}N\tilde{f}^t \kappa\delta^{tt'}\tilde{f}^{t'} \\ -\tilde{h}^t (w\delta^{tt'}\Phi^{t-1,t'-1})\tilde{h}^{t'} \end{pmatrix} \begin{pmatrix} -\frac{1}{2}\tilde{h}^t (u\mathbb{X}^{t-1,t'-1})\tilde{h}^{t'} \end{pmatrix} \\
& \stackrel{8}{=} \int_{\Phi\tilde{C}} \exp \left\{ -N\tilde{C}^{tt'}\Phi^{tt'} \right\} \exp \left\{ \begin{array}{l} -\frac{1}{2}y^t ((v\Phi^- + \kappa)^{-1})^{tt'} y^{t'} \\ \phi^t \tilde{C}^{tt'}\phi^{t'} \end{array} \right\} \begin{pmatrix} -\frac{1}{2}y^t ((v\Phi^- + \kappa)^{-1})^{tt'} y^{t'} \\ -\frac{1}{2}h^t ((w\Phi^- + u\mathbb{X}^-)^{-1})^{tt'} h^{t'} \end{pmatrix} \begin{pmatrix} -\frac{1}{2}\ln |\frac{1}{N}(v\Phi^- + \kappa)| \\ -\frac{1}{2}\ln |w\Phi^- + u\mathbb{X}^-| \end{pmatrix} \\
& \stackrel{9}{=} \int_{\Phi\tilde{C}} \exp \left\{ N[-\tilde{C}^{tt'}\Phi^{tt'} - \ln Z(\tilde{C}; \Phi)] \right\}
\end{aligned}$$

Herein, we made the following manipulations:

1. Rewrite each Dirac delta enforcing the deterministic network equations in its Fourier representation,  $\delta(\circ) = \int d\tilde{z} \exp\{\iota\tilde{z}(\circ)\}$ , introducing conjugate fields  $\tilde{f}^t, \tilde{h}^t$  for the outputs  $y^t$  and hidden pre-activations  $h^t$ . This converts the constraints into linear couplings in the exponent, such that all random variables only appear in the equation through quadratic forms.
2. Integrate out the Gaussian weight priors  $\{\mathbf{W}^{(t)}\}_t, \mathbf{U}, \mathbf{V}$  and the output noise  $\xi$ . We introduce the variable  $\bar{\delta}^{tt'}$

$$\bar{\delta}^{tt'} := \begin{cases} \delta^{tt'}, & \text{DNN} \\ 1, & \text{RNN} \end{cases}$$

which allows us to write down the covariance of the priors in the short form  $\langle \mathbf{W}_{ij}^{(t)} \mathbf{W}_{ij}^{(t')} \rangle = W \delta^{tt'}$  (and analogously for  $U, V, \kappa$ ). We denote the corresponding masking operator on time indices by

$$(\llbracket A \rrbracket)^{tt'} := \bar{\delta}^{tt'} A^{tt'},$$

which acts as a diagonal projector in  $t, t'$  for DNNs and as the identity for RNNs.

3. Introduce the empirical kernel  $\Phi^{tt'} := \frac{1}{N} \sum_{i=1}^N \phi_i^t \phi_i^{t'}$  via a Dirac delta,  $\delta(\Phi - \frac{1}{N} \sum_i \phi_i \phi_i) = \int d\tilde{C} \exp \left\{ \tilde{C}^{tt'} \left( \Phi^{tt'} - \frac{1}{N} \sum_i \phi_i^t \phi_i^{t'} \right) \right\}$ , in order to decouple different neurons. The  $\int d\tilde{C}$  integral is taken along a contour parallel to the imaginary axis passing through the saddle point; we omit an explicit imaginary unit, anticipating that the saddle lies on the real axis. As long as there are no singularities between the original and shifted contours, such deformations are justified (Bromwich contour).

4. Rescale the output conjugate field according to  $\tilde{f} \mapsto N\tilde{f}$  so that its quadratic form scales as  $\mathcal{O}(N)$ , on the same footing as the contribution from the hidden conjugate fields. This is an algebraic change of variables that prepares the expression for a uniform large- $N$  analysis.
5. Exploit the fact that now, conditional on the collective fields  $(\Phi, \tilde{C})$ , different neurons are independent and identically distributed. This allows us to factor the  $N$ -dimensional integral over  $\{h_i, \tilde{h}_i\}_{i=1}^N$  into a product of identical single-site integrals.
6. Rescale the conjugate kernel to make the overall  $N$ -dependence explicit,  $\tilde{C} \mapsto N\tilde{C}$ . After this redefinition the kernel term in the exponent takes the canonical form  $-\frac{N}{2}\tilde{C}^{tt'}\Phi^{tt'}$ , so that the full effective action is proportional to  $N$ .
7. Insert the mean-field ('intensive') scalings for the prior variances, e.g.  $V = v/N^2$ ,  $W = w/N$ ,  $U = u/N$  (and similarly for the noise level), so that the pre-activation covariances and outputs remain of order one as  $N \rightarrow \infty$ . This yields quadratic forms involving  $v, w, u$  and the kernels  $\Phi$  rather than the original extensive parameters.
8. Perform the remaining Gaussian integrals over  $\tilde{f}$  and over the hidden fields (after integrating out their conjugate fields inside the single-site factor). This produces the quadratic form in the outputs  $y$ , with covariance  $v\Phi^- + \kappa$ , as well as the corresponding log-determinant normalization, and an analogous Gaussian contribution for the hidden fields involving the matrix  $w[\Phi^-] + u\mathbb{X}^-$ .
9. Recognize that the contribution of a single neuron is captured by a partition function  $Z(\tilde{C}; \Phi)$  which only depends on the collective fields through  $(\Phi, \tilde{C})$ . Because all neurons are identically distributed, the full factor from the hidden layer is  $Z(\tilde{C}; \Phi)^N$ , which yields a term  $-N \ln Z(\tilde{C}; \Phi)$  in the effective action.
10. Apply a saddle-point approximation (Laplace's method) to the remaining functional integral over  $(\Phi, \tilde{C})$  in the limit of large width  $N$ . The exponent is of the form  $N S(\Phi, \tilde{C})$ , so the integral is dominated by the stationary points of  $S$ ; this is equivalent to invoking a large-deviation principle for the empirical kernel.

A key object that arises from this calculation is the single-site cumulant generating function

$$W(\tilde{C}; \Phi) = \ln Z(\tilde{C}; \Phi) = \ln \int_{h\tilde{h}} \exp \left\{ -\phi^t \tilde{C}^{tt'} \phi^{t'} - \frac{1}{2} h^t ((w[\Phi^-] + u\mathbb{X}^-)^{-1})^{tt'} h^{t'} - \frac{1}{2} \ln |w[\Phi^-] + u\mathbb{X}^-| \right\}. \quad (46)$$

whose derivatives with respect to  $\tilde{C}$  yield the cumulants  $\phi\phi^T$ .

## A.8. Additional figures

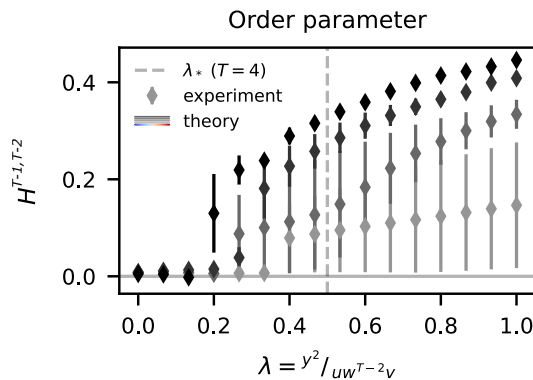


**Figure A.6.** Like Fig. 3, but with nonlinear activation  $\phi(\circ) = \text{erf}(\frac{\sqrt{\pi}}{2}\circ)$ .